Bachelor Project

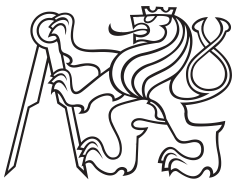

Czech
Technical
University
in Prague

F3

Faculty of Electrical Engineering
Department of Cybernetics

Sources of Transmission Localization by a Formation of Helicopters Equipped by a Rotating Directional Antenna

Václav Pritzl

Supervisor: Ing. Martin Saska, Dr. rer. nat.
Field of study: Cybernetics and Robotics
Subfield: Robotics
May 2018

BACHELOR‘S THESIS ASSIGNMENT

I. Personal and study details

Student's name: **Pritzl Václav** Personal ID number: **456894**

Faculty / Institute: **Faculty of Electrical Engineering**

Department / Institute: **Department of Cybernetics**

Study program: **Cybernetics and Robotics**

Branch of study: **Robotics**

II. Bachelor’s thesis details

Bachelor’s thesis title in English:

Sources of Transmission Localization by a Formation of Helicopters Equipped by a Rotating Directional Antenna

Bachelor’s thesis title in Czech:

Lokalizace zdrojů vysílání formací helikoptér vybavených otočnou směrovou anténou

Guidelines:

The goal of the thesis is to design, implement, and experimentally verify in Gazebo simulator and real experiments an application for localization of sources of transmission (e.g. ARFID tags) by a formation of an Unmanned Aerial Vehicles (UAVs) equipped with a rotating directional antenna. The following tasks will be solved:
1. To design and implement a technique for localization of ARFID tags by combining results of estimation of their relative positions from multiple UAVs (using 1. distance depending on measured intensity and 2. bearing based on antenna orientation).
2. To design and implement a method for effective (fast and precise) ARFIDs localization by a formation of relatively localized UAVs, taking advantage of possibility to reactively change scale and position of the formation.
3. To integrate the methods into the ROS system being designed at MRS group, CTU in Prague [1,2].
4. To verify system functionalities in Gazebo and with real platforms in outdoor conditions.
5. To statistically compare and discuss achieved results with a system using omnidirectional antennas and with a system using static directional antennas (the UAV itself is rotating).

Bibliography / sources:

[1] T. Baca, P. Stepan and M. Saska. Autonomous Landing On A Moving Car With Unmanned Aerial Vehicle. In The European Conference on Mobile Robotics (ECMR), 2017.
[2] G. Loianno, V. Spurny, J. Thomas, T. Baca, D. Thakur, D. Hert, R. Penicka, T. Krajnik, A. Zhou, A. Cho, M. Saska, and V. Kumar. Localization, Grasping, and Transportation of Magnetic Objects by a team of MAVs in Challenging Desert like Environments. IEEE ICRA and RAL, 2018.
[3] V. Kumar, N. Michael. Opportunities and challenges with autonomous micro aerial vehicles. The International Journal of Robotics Research. Vol 31, Issue 11, pp. 1279 - 1291, 2012.
[4] S. J. Julier and J. K. Uhlmann. A New Extension of the Kalman Filter to Nonlinear Systems. In Proc. of AeroSense: The 11th Int. Symp. On Aerospace/Defence Sensing, Simulation and Controls, 1997.
[5] J. Rodas, T. M. Fernandez, D. I. Iglesia, C. J. Escudero. Multiple Antennas Bluetooth System for RSSI Stabilization, in Wireless Communication Systems, 2007.

Name and workplace of bachelor's thesis supervisor:

Ing. Martin Saska, Dr. rer. nat., Multi-robot Systems, FEE

Name and workplace of second bachelor's thesis supervisor or consultant:

Date of bachelor's thesis assignment: **12.01.2018** Deadline for bachelor thesis submission: **25.05.2018**

Assignment valid until: **30.09.2019**

Ing. Martin Saska, Dr. rer. nat.	doc. Ing. Tomáš Svoboda, Ph.D.	prof. Ing. Pavel Ripka, CSc.
Supervisor's signature	Head of department's signature	Dean's signature

III. Assignment receipt

The student acknowledges that the bachelor's thesis is an individual work. The student must produce his thesis without the assistance of others, with the exception of provided consultations. Within the bachelor's thesis, the author must state the names of consultants and include a list of references.

.	
Date of assignment receipt	Student's signature

Acknowledgements

I would like to thank my supervisor Martin Saska for his guidance during my work on this thesis. Furthermore, I would like to thank all the people from Multi-robot Systems group, namely Tomáš Báča, Vojtěch Spurný and Matouš Vrba, for their help with the experiments, ROS and other problems I have dealt with during the work on this thesis. I would especially like to thank my family for supporting me during my studies. Finally, I would like to thank my friend Adam Kollarčík for his endless supply of motivating words during my work on this thesis.

Declaration

I declare that the presented work was developed independently and that I have listed all sources of information used within it in accordance with the methodical instructions for observing the ethical principles in the preparation of university theses.

Prague, 24. May 2018

Abstract

This thesis proposes a novel technique for radio frequency (RF) transmission sources localization in outdoor environments using a formation of autonomous Micro Aerial Vehicles (MAVs) equipped with a rotating directional antenna. Precise localization of sources of transmission is required in numerous defense, security, industry, and civil applications. The proposed technique uses a fusion of RSSI and angle of arrival (AoA) data gained from measured radiation patterns of a variable number of directional antennas mounted on each MAV in order to reliably determine targets positions. A UKF-based approach is then used for sensor data fusion and for estimation of targets positions during each localization step. The MAV formation actively reacts to current position estimate and repositions itself to achieve optimal localization results. The proposed method has been verified in simulations of noisy and inaccurate measurements in the Gazebo robotic simulator. The performance of the proposed approach has been further evaluated in several successful real-world outdoor deployments of the system employing multiple cooperatively working MAVs equipped with a rotating directional antenna connected to XBee wireless device.

Keywords: RFID localization, micro aerial vehicles, unscented kalman filter, directional antenna, radio frequency transmission sources localization

Supervisor: Ing. Martin Saska, Dr. rer. nat.

Abstrakt

Tato práce se zabývá novou technikou lokalizace zdrojů radiového vysílání ve venkovních prostorech pomocí formace bezpilotních helikoptér vybavených otočnou směrovou anténou. Přesná lokalizace zdrojů radiového vysílání má uplatnění v mnoha oblastech, ať už jde o použití v obraně, zabezpečení, průmyslu nebo běžném životě. Metoda navržená v této práci využívá kombinaci údajů o intenzitě a úhlu příchozího signálu, získaných z naměřených směrových charakteristik proměnlivého počtu směrových antén připevněných na každé použité helikoptéře. Pro fúzi dat a odhad polohy hledaného objektu je v každém kroku lokalizace použit Unscented Kalman Filter. Formace helikoptér aktivně reaguje na aktuální odhad polohy a upravuje svou polohu pro dosažení optimálních výsledků lokalizace. Funkčnost navržené metody byla ověřena v simulacích zašuměných a nepřesných dat v robotickém simulátoru. Chování algoritmu bylo dále otestováno v několika úspěšných reálných pokusech se systémem několika spolupracujících helikoptér vybavených otočnou směrovou anténou připojenou k radiovému modulu XBee.

Klíčová slova: RFID lokalizace, bezpilotní helikoptéry, Kalmanův filtr, směrová anténa, lokalizace zdrojů radiového vysílání

Překlad názvu: Lokalizace zdrojů vysílání formací helikoptér vybavených otočnou směrovou anténou

Contents

Figures

Chapter 1

Introduction

Fast and precise radio frequency (RF) transmission sources localization is a challenging task utilized in many different fields and industries. Active radio frequency identification (RFID) chips are commonly used in many industrial applications, such as finding working tools or machinery in construction sites or localization and identification of stock items in warehouses. Likewise, an RF beacon can be connected to a sensor that wishes to establish a high-rate data link. Similarly, RFID can be conveniently used in agriculture for livestock tracking in order to monitor cattle health, prevent cattle rustling or localize lost animals. Tracking of endangered species is another widespread use of RFID chips. Furthermore, RF localization brings an undeniable benefit to searching for people during natural disasters or search and rescue operations (such as localizing people in avalanches using special RF devices or looking for missing people by tracking their mobile phones). Military applications include localizing wounded soldiers on the battlefield or using RF localization to substitute the GPS system in case of GPS jamming or operating in indoor spaces. In all of these cases, the speed, precision, and reliability of the localization are extremely important.

The use of Micro Aerial Vehicles (MAVs) has recently experienced a great surge in popularity and new applications for MAV use emerge every day. Because of their ability to quickly reach distant or dangerous places, the possibility to carry various sensors, devices and cargo, and their easy accessibility, they quickly found their use for example in terrain mapping, delivery of cargo, photography and video recording, surveillance and manipulation of objects. Their abilities also make them ideal for utilization in RF localization.

There are many different approaches to RF localization with variable requirements in terms of needed infrastructure and cost of required equipment and with variable localization speed and precision. This thesis proposes a localization method which uses combined Received Signal Strength Indication (RSSI) and Angle of Arrival (AoA) data obtained from directional antennas mounted on multiple MAVs flying in a close formation. This approach enables the use of cheap and easily available sensors and utilizes the ability of an MAV formation to quickly change its position and shape in order to quickly and precisely determine the position of the localized object without the need of a long preparation.

This thesis is built upon previous research conducted at Multi-robot Systems group at Czech Technical University, Department of Cybernetics. The thesis [1] deals with the topic of RF localization using RSSI data, Bluetooth Low Energy (BLE) technology and Extended Kalman Filter (EKF). The proposed approach has been proven to work but the used technology had low range and the method was susceptible to RSSI measurement disturbance and multipath effects. In [2] a combined UKF and trilateration approach is used for localization from RSSI data measured by Xbee 2.4 GHz devices and an adaptive formation control algorithm for localization is proposed. In [3] the aforementioned approaches are described along with more experiments and an AoA approach which uses a directional antenna and a Weighted Robust Least Squares method. Furthermore, this thesis builds upon previous research on MAV formation control [4] [5] and relative localization [6] [7].

1.1 State of the Art

The utilization of MAVs and other mobile robot systems for RF localization has already been explored multiple times in literature and a number of different approaches exist.

The simplest approach is the use of RSSI values measured by a simple omnidirectional antenna. This method requires no complicated infrastructure or sensors and cheap and easily available RF devices are enough to produce results using this method. However, it requires knowledge of parameters of signal propagation in the given environment and if used on its own it is susceptible to radio disturbance, multipath effects, shadowing and other effects influencing radio transmission propagation.

This method is explored in [8] which deals with the use of MAVs in RFID

localization for environmental monitoring. Specifically, it uses an RSSI-based multilateration approach, which estimates the position of the localized chip using a least-squares method. [9] researches the use of a particle filter on RSSI data measured by a UAV sweeping a large outdoor area. Similarly, [10] proposes a method for Wi-Fi devices localization in a large region using UAVs to collect RSSI data. A Bayesian optimization based on Gaussian process regression is then used for the localization itself. In [11], tracking of an intermittent RF source using a UAV swarm measuring RSSI data is researched. Two algorithms for localization are compared - EKF and a recursive Bayesian estimator. Furthermore, the paper compares two trajectory planning algorithms for RF localization - steepest descent posterior Cramer-Rao lower bound path planning and a bio-inspired heuristic path planning.

Another possible approach is the use of AoA information estimated from the radiation pattern of a directional antenna. This approach is used in [12], where a directional antenna is mounted on top of an MAV, which rotates around its vertical axis, and a particle filter is used for RF source localization. In [13], autonomous navigation of a mobile ground robot to an RF source using AoA information and a particle filter is explored. Similarly, directional RSSI-based localization using a mobile robot carrying a corner reflector antenna and an online statistical filter is researched in [13].

In order to decrease the influence of multipath effects on successful localization, the aforementioned approaches can be combined and used together (as is the case with this thesis). In [14] and [15], methods for localization in Non Line of Sight condition from coupled RSSI and AoA measurements using a particle filter and a multi-step Gaussian filtering approach, respectively, are proposed.

A more precise method is the use of Time Difference of Arrival (TDoA), which is based on the measurement of the difference in time between the arrival of the transmission to multiple receivers. This approach is accurate and resistant to multipath effects but requires more complicated devices. RF localization using TDOA measurements from 2 UAVs and a comparison of an EKF and UKF approach are described in [16]. Similarly, [17] proposes a dual-EKF algorithm used to localize an RF emitter from TDoA data measured by two UAVs. [18] proposes a TDOA-based method utilizing a least squares approach for localization using UAVs in battlefield environments as a substitute for Global Navigation Satellite Systems (GNSS).

1.2 Problem Statement

The localization system in its basic form consists of three autonomous cooperatively working MAVs flying in a formation and of a variable number of beacons to be localized. Positions of the beacons are completely unknown beforehand. The beacons are active RFID chips capable of communication with directional antennas mounted on each MAV.

The antennas are able to send a message to each beacon and measure RSSI of the beacon's response. The antenna is able to rotate itself to a specific position around its vertical axis and using this feature it is possible to measure the current radiation pattern of the antenna in 360 degrees. Using this measured radiation pattern it is possible to estimate distance and angle (bearing) between each MAV and the beacon currently being localized. The environment where the localization is performed is assumed to be without obstacles which eliminates the influence of shadowing on transmission propagation.

For purpose of the localization, it is further assumed that the beacon is placed on the ground, at zero altitude, which reduces the localization task to two dimensions. This simplification is made because bearing information is independent of beacon's altitude and dependence of transmission RSSI on distance is on its own too influenced by radio disturbance and multipath effects to be able to reliably determine beacon's altitude. Furthermore, the estimation of beacon's altitude is not required by the possible applications of this method (as listed in Chapter 1).

Moreover, it is assumed that positions of the MAVs are accurately known, e.g. using GPS. The goal of this work is to reliably and precisely estimate the current position of each beacon using information obtained from each antenna and position of each MAV.

Chapter 2

Used hardware description

2.1 MAV platform

MAV platforms built by the CTU Multi-robot System group were used in the experiments. Each used MAV is a hexacopter controlled by a Pixhawk[1] unit running Robot Operating System[2] (ROS). Real-time kinematic (RTK) positioning in combination with Global Navigation Satellite System (GNSS) is used in order to get high-precision position data for each MAV. Every MAV offers approximately 15 minutes of flight time depending on flight conditions. The real world experiments were performed either with the use of a single drone or a formation of 3 MAVs. More information about the used MAV hardware can be found in [19] and [20]. Information about the Model Predictive Control (MPC) used to control the MAVs can be found in [21], and [22]. The MAVs use a decentralized collision avoidance system [23] in order to enable a safe execution of real experiments.

2.2 Beacon description

XBee S2C radio module with an integrated wire antenna shown in Figure 2.1a is used as the localized beacon. XBee modules are used in a number

[1] `https://pixhawk.org/`
[2] `http://www.ros.org/`

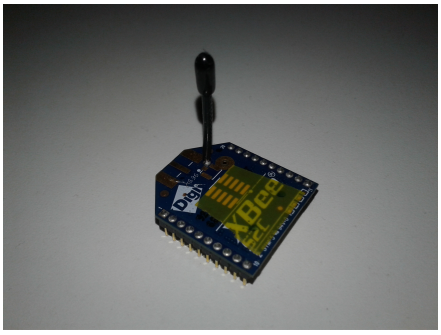

(a) : XBee S2C RF module

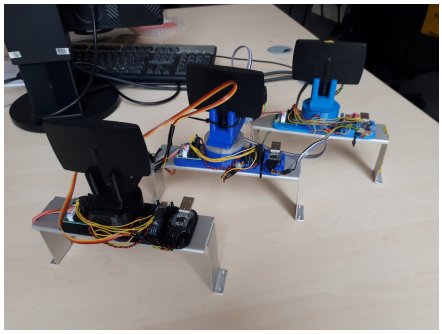

(b) : Rotating antennas used for localization

Figure 2.1: Hardware used for localization

Specification	Value
Indoor/urban range	Up to 60 m
Outdoor RF line-of-sight range	Up to 1200 m
Transmit power output (maximum)	3.1 mW (+5 dBm), normal mode
Receiver sensitivity	-100 dBm, normal mode
Supply voltage	2.2 V - 3.6 V
Operating frequency band	ISM 2.4 - 2.5 GHz

Table 2.1: Technical specifications of XBee S2C module

of various applications ranging from receiving data from wireless sensors to remote control of mobile robots. Technical specifications of XBee S2C module can be found at[3], while a summary is included in Table 2.1.

During collection of each sample to be used for localization, the antenna transmits a short message to the beacon and the beacon responds. Measured RSSI of the received response is then used by the localization algorithm.

2.3 Antenna description

The receiver was designed by Matouš Vrba from Multi-robot Systems group at CTU within his work on RFID chips localization [3]. Two more antenna devices were constructed for the purpose of this thesis by its author. All three antennas can be seen in Figure 2.1b. The antenna rotating device consists of XBee S2C module with a CW8DPA patch directional antenna connected to XBee via RP-SMA connector. The antenna gain is 8 dBi and its operating

[3] `https://www.digi.com/resources/documentation/digidocs/pdfs/90002002.pdf`

Figure 2.2: MAV with directional antenna

frequency band is 2.4 - 2.5 GHz.

The antenna and RF module are mounted on a 28BYJ-48 step motor that is used for rotating the antenna. An Arduino Nano is used to control the step motor. The step motor is capable of rotating the antenna to 128 different positions which equals a step of approximately 2.8°. The Xbee device is connected to a CP2102 USB to UART converter. USB ports are then used to connect the XBee and the step motor to the MAV control unit. For localization purposes, the antenna is mounted below the MAV as can be seen in Figure 2.2.

Chapter 3

System model

State-space representation of the localization system is defined in Section 3.1. The equations used for modeling the dependency of RSSI on the distance between localized beacon and each antenna are described in Section 3.2. The estimation of angle of arrival (AoA) of the signal to the respective directional antenna is described in Section 3.3.

3.1 State-space representation of system

A discrete state-space model of the localization system for m MAVs and one beacon is used as

$$\vec{x}_{k+1} = \mathbf{A}\vec{x}_k + \vec{v}_k, \tag{3.1}$$

$$\vec{z}_k = \vec{h}(\vec{x}_k, \vec{u}_k) + \vec{w}_k, \tag{3.2}$$

where $\vec{x}_k$ is the 2-dimensional state of the system at timestep k containing Cartesian coordinates of the localized beacon (the localization task has been reduced to two dimensions as described in Section 1.2), $\vec{v}_k$ is the state noise process vector, $\vec{z}_k$ is the observation vector, $\vec{h}$ is the measurement function, $\vec{u}_k$ is the input vector containing x, y and z coordinates of the currently used MAV and $\vec{w}_k$ is the measurement noise. Matrix $\mathbf{A}$ is a 2-dimensional identity matrix which represents that position of the localized beacon is static.

$$\mathbf{A} = \begin{bmatrix} 1 & 0 \\ 0 & 1 \end{bmatrix} \tag{3.3}$$

The process and measurement noise vectors are defined as

$$\vec{v}_k \sim \mathcal{N}(0, \mathbf{Q}_k),$$

$$\vec{w}_k \sim \mathcal{N}(0, \mathbf{R}_k),$$

where $\mathbf{Q}_k$ is the process noise covariance matrix and $\mathbf{R}_k$ is the measurement noise covariance matrix. The state vector, input vector and measurement vector are defined as

$$\vec{x}_k = [x_B, y_B]^T,$$

$$\vec{u}_k = [x_M, y_M, z_M]^T,$$

$$\vec{z}_k = [RSS, \theta]^T,$$

where x_B and y_B denote the Cartezian coordinates of the localized beacon. x_M, y_M, z_M are the coordinates of the MAV whose sensor data are currently used for localization. RSS is the average RSSI of the radiation pattern measured by the MAV and θ is the estimated AoA obtained from the MAV. The measurement function is defined as

$$\vec{h} = \begin{bmatrix} P_0 - 10\gamma \log_{10}(\sqrt{(x_M - x_B)^2 + (y_M - y_B)^2 + (z_M - z_B)^2}) \\ \text{atan2}(y_B - y_M, x_B - x_M) \end{bmatrix}.$$

where atan2 is the four-quadrant inverse tangent defined as

$$\text{atan2}(x, y) = \begin{cases} \arctan(\frac{y}{x}) & \text{if } x > 0 \\ \arctan(\frac{y}{x}) + \pi & \text{if } x < 0 \text{ and } y \geq 0 \\ \arctan(\frac{y}{x}) - \pi & \text{if } x < 0 \text{ and } y < 0 \\ +\frac{\pi}{2} & \text{if } x = 0 \text{ and } y > 0 \\ -\frac{\pi}{2} & \text{if } x = 0 \text{ and } y < 0 \\ \text{undefined} & \text{if } x = 0 \text{ and } y = 0. \end{cases}$$

The first row of the measurement function vector contains RSSI calculation from 3D distance between the beacon and the MAV according to equation (3.7) and the second row of the function contains calculation of estimated MAV-beacon angle from position of the beacon and the MAV. It can be seen that the measurement function is highly nonlinear which highlights the necessity of using a type of Kalman filter designed for nonlinear systems.

The localization system contains m MAVs, each passing measured data to the filter in every position of measurement. The measured data (vectors $\vec{u}_k$ and $\vec{z}_k$) are passed to the filter sequentially resulting in m filter steps for every formation measurement position.

3.2 Signal strength model

Friis transmission equation (3.4) describes the dependency of received signal strength on certain properties of transmitter and receiver and on the distance between them under ideal conditions. Power P_r received by the antenna in decibel-milliwatts (dBm) can be obtained as

$$P_r = P_t + D_t + D_r + 20\log_{10}(\frac{\lambda}{4\pi d}), \tag{3.4}$$

where P_t is the power delivered to the transmitter in dBm, D_t is transmitting antenna isotropic gain in the direction of the receiver antenna in decibels isotropic (dBi), D_r is receiver antenna isotropic gain, λ is the transmission wavelength in meters, and d is the euclidean distance between transmitter and receiver in meters.

This idealized equation applies only under certain conditions. It is assumed that $d << \lambda$ which means that both the receiving and transmitting antenna are in each other's far field. Furthermore, both antennas must be correctly aligned and equally polarized. The equation does not account for any multipath effects caused by signal reflection from the ground and obstacles, shadowing and other propagation effects occurring under real-world conditions. A brief summary of effects influencing the transmission propagation can be found at [24]. To account for these influences the Log-distance path loss model

$$PL(d) = \overline{PL}(d_0) + 10\gamma\log_{10}(\frac{d}{d_0}) + \chi \tag{3.5}$$

is used. The Received signal strength then equals

$$P_r = P_t - PL \tag{3.6}$$

where P_r is the power received by the receiver antenna in dBm, and P_t is the power delivered to the transmitting antenna. $PL(d)$ is the path loss in dB at distance d, $\overline{PL}(d_0)$ is the mean path loss at reference distance d_0 and γ is the path loss exponent. $\chi \in (0, \sigma^2)$ is normally (Gaussian) distributed random variable with zero mean and standard deviation σ that represents the effects of multipath, shadowing and radio disturbance on the transmission. By combining equation (3.6) and (3.5) and substituting $d_0 = 1$ a dependency

$$P_r = P_0 - 10\gamma\log_{10}(d) + \chi \tag{3.7}$$

of RSSI P_r on distance d between transmitter and receiver which contains two parameters P_0 and γ is obtained. These parameters depend on transmitter and receiver properties and on the environment where the signal spreads and can be experimentally identified by measuring the dependency of RSSI on transmitter-receiver distance and fitting the function (3.7) to the data using a least squares method.

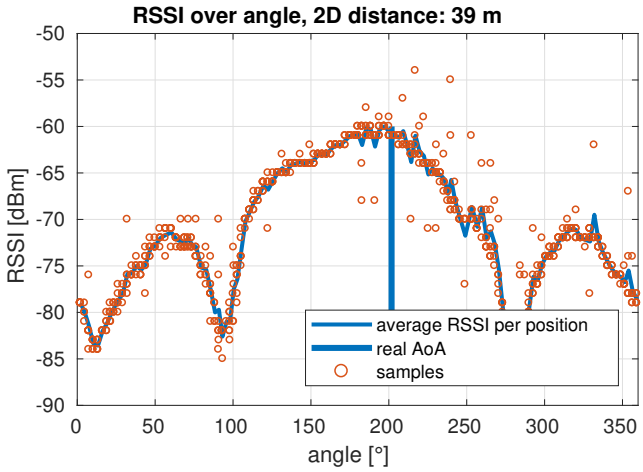

Figure 3.1: Radiation pattern measured on MAV 39 m away from the beacon and 3.5 m above the ground.

3.3 Antenna radiation pattern and MAV-beacon bearing

Antenna radiation pattern refers to a mathematical function or a graphical representation of the radiation properties of the antenna as a function of space coordinates [25], which is mostly represented as a function of the directional coordinates. A 2D radiation pattern cut can be measured by rotating the antenna around a fixed axis and measuring received/transmitted power in a particular direction. Portions of the radiation pattern bounded by regions of relatively weak radiation intensity are called radiation lobes. Usually, they are subclassified into main, side and back lobes. The main lobe is defined as "the radiation lobe containing the direction of maximum radiation"[25]. A directional antenna is defined as an antenna which radiates or receives greater power in specific directions. An important property of the antenna is called gain in dBi (decibels isotropic). It represents the ratio of the radiation intensity in a given direction to the radiation intensity of a lossless isotropic antenna (radiating equally in all directions). Specifically, the antenna used in this thesis has a gain of 8 dBi in the direction of the main lobe. An example of a measured radiation pattern can be found in Figure (3.1).

The angle θ representing the bearing from the particular antenna to the beacon being localized can be estimated from the location of the main lobe in the measured horizontal radiation pattern cut. The angle θ is defined as the horizontal angle in the x-y plane, $\theta = 0$ corresponds to positive half of the x axis, and θ is positive in the direction of the positive half of the y axis.

Chapter 4

Localization algorithm with uncertainty estimation

A localization algorithm with a novel approach to uncertainty estimation will be proposed in this chapter. The localization algorithm accepts RSSI data measured by the directional antenna along with information about the bearing where the current RSSI was measured as described in Section 4.1. A radiation pattern is constructed from a set of these measurements. This pattern is then preprocessed, used for calculation of average RSSI of the whole pattern and estimation of transmission AoA as described in Section 4.2. Furthermore, an uncertainty of this AoA estimation is calculated using algorithm shown in Section 4.3. Unscented Kalman filter described in Section 4.4 is then used to estimate the position of the localized beacon.

4.1 Radiation pattern measurement

The radiation pattern of the antenna, described in Section 3.3, is measured by using the step motor to rotate the antenna in 360 degrees sampled into 128 positions around its z axis. In every position, several RSSI samples are measured. From the performed experiments, it became clear that the frequency of measured samples varies substantially. Therefore, the antenna waits for a certain number of samples in each position set by the step motor. Six samples per position were used during the real experiments as a compromise between filtering as much random noise as possible and doing as quick measurements as possible. Furthermore, the time spent in each

position is limited by a timeout value to prevent the antenna from freezing in a position where no transmission can be established. This timeout value was set to 400 ms per position. The first position was set to have a larger timeout of 2 s in order to give the antenna more time to establish communication. Another approach to measuring the radiation pattern is rotating the whole MAV while the antenna's rotation relative to the MAV does not change. This approach is described in Section 5.1.

4.2 Preprocessing of measurements

As mentioned before, the rotating antenna measures several samples in each of 128 different rotations around its z axis in order to decrease the influence of multipath propagation and other effects that cause random noise in the measured RSSI. An average of the measured samples in each position is then computed. The average RSSI per position k is calculated from n samples using arithmetic mean described in equation (4.1) and the calculation of the average angle is shown in equation (4.2). Although the samples are taken in the same rotational position of the antenna, the angle can vary due to changes in yaw of the whole MAV.

$$\overline{RSS}_k = \frac{1}{n}(\sum_{i=1}^{n} RSS_{ki}) \tag{4.1}$$

$$\overline{\alpha}_k = \text{atan2}(\sum_{i=1}^{n} \text{sin}\alpha_{ki}, \sum_{i=1}^{n} \text{cos}\alpha_{ki}) \tag{4.2}$$

In case a static directional antenna is used (the MAV itself rotates in 360 degrees around its z axis), the approach of beacon position estimation stays unchanged. The whole rotation is sampled into 128 positions and the average values are calculated using the same equations for each particular angle step.

The computed RSSI values are then used to calculate the average RSS of whole radiation pattern which is further used by the UKF for estimating the beacon position.

Even after the measurement of multiple samples in each position the measured pattern still contains an unacceptable amount of noise. To solve this issue, a simple moving mean is used to further filter the data. A moving mean, that uses n values, iterates through the data and for every position computes an average of $\frac{n}{2}$ previous positions, current position, and $\frac{n}{2}$ subsequent positions. Furthermore, the moving mean fills in the missing data in case there were no samples measured in a given position but the

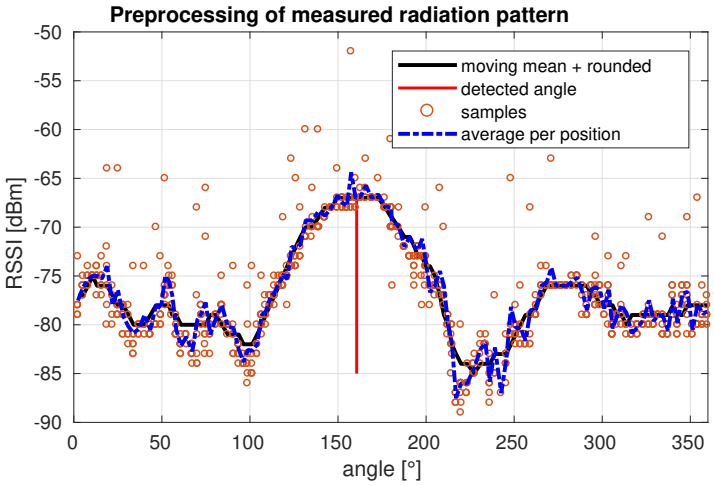

Figure 4.1: Preprocessing of measured radiation patterns

surrounding positions have been measured correctly. By analyzing the data obtained from experiments, $n = 7$ samples were chosen as the appropriate value to be used by the moving mean in each calculation step.

The RSSI values are rounded to whole decibels. Because of this, similar RSSI values are treated as equal during the search for the angle with maximal RSSI and the algorithm will choose the average of these angles rather than one angle with a little higher RSSI than the others. This usually means choosing an angle closer to the center of the main lobe which improves the estimation accuracy. An example of a measured radiation pattern with results after each preprocessing step can be seen in Figure 4.1.

The transmission AoA is then determined from this preprocessed radiation pattern. The algorithm simply finds the angle with maximal RSSI in the data. In case that multiple positions share the same maximal RSSI, the average angle of these positions is calculated using equation (4.2) and returned as the desired AoA.

4.3 Uncertainty of angle measurement estimation

After preprocessing the measured radiation pattern and estimating the angle of arrival, an uncertainty of the current AoA measurement is estimated from the shape of the radiation pattern. It serves as a weight of the measurement in localization and is further used for determining whether the measurement should be used in localization and then for construction of the measurement

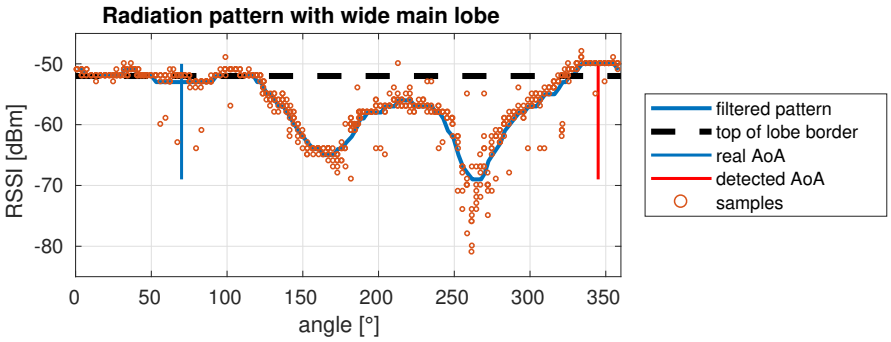

Figure 4.2: Radiation pattern with wide main lobe

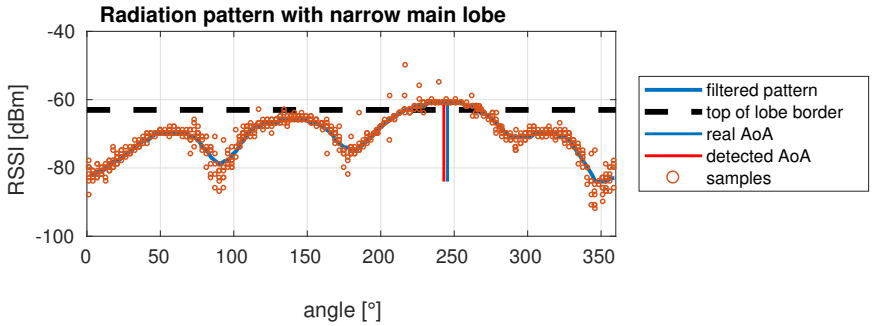

Figure 4.3: Radiation pattern with narrow main lobe

noise matrix $\mathbf{R}$.

This uncertainty σ_θ is calculated by finding the value that is furthest away from the angle with maximal RSSI at the level of 2 dBm below maximal RSSI value and calculating the subtraction of these angles. This effectively means cutting the top of the radiation pattern and finding the width of the section between the edge of the top and the estimated AoA. Examples of measured radiation patterns with plotted border of the 2 dBm radiation pattern top can be seen in Figures 4.2 and 4.3. The first figure contains a radiation pattern with a very wide main lobe where the AoA estimation from maximal RSSI failed to produce an accurate result. However, due to the width of radiation pattern section above the plotted border, the weight of this measurement is low. In the second figure, a radiation pattern with a narrow main lobe and an accurate estimation of AoA is displayed. A large weight has been assigned to this measurement.

The 2 dBm height of the radiation pattern top has been determined from data obtained in real experiments in order to optimally estimate the credibility of the measurements. By using a Student's t-test, a correlation has been found between the estimated angle uncertainty and the error in AoA estimation. The correlation coefficient between the estimated angle uncertainty vector

and the AoA error vector is defined as

$$R_{\vec{X},\vec{Y}} = \frac{\sum_{j=1}^{n}(X_j - \bar{X})(Y_j - \bar{Y})}{\sqrt{(\sum_{j=1}^{n}(X_j - \bar{X})^2)(\sum_{j=1}^{n}(Y_j - \bar{Y})^2)}}, \tag{4.3}$$

where $\vec{X}$ is the estimated angle uncertainty vector, $\vec{Y}$ is the real angle estimation error vector, and $\bar{X}$, $\bar{Y}$ are means of these vectors. This correlation coefficient is calculated in Chapter 7 for data gained from experiments to verify the usefulness of estimating the angle uncertainty for every measurement as opposed to choosing a constant parameter for all steps. Student's t-test [26] was used to calculate statistical significance of the discovered correlation.

The estimated AoA uncertainty is further used to determine whether the measurement should be used by the UKF for localization. If the uncertainty is larger than 3 radians, the algorithm throws the measurement away and does not perform a filter step. This eliminates the measurements with very large uncertainty which would decrease the filter performance.

Furthermore, the AoA uncertainty is used to construct the measurement noise $\mathbf{R}$ matrix constructed as

$$\mathbf{R} = \begin{bmatrix} \sigma_{RSS}^2 & 0 \\ 0 & \sigma_{\theta}^2 \end{bmatrix}.$$

The covariance between average RSSI and AoA measurement noise is assumed to be zero and therefore $\mathbf{R}$ is a diagonal matrix. The average RSSI standard deviation σ_{RSS} is a constant value identified from the performance of the filter on real experimental data while estimated AoA uncertainty σ_{θ} is changed in every step.

4.4 Unscented Kalman filter

Kalman filter (KF), described e.g. in [27], was used to fuse the measured data from all MAVs and estimate the position of the localized beacon. KF is a simple and robust state estimator algorithm with low computational requirements which is proper for onboard use on MAV hardware. Due to nonlinearities in the system model described in Section 3.1 a version of KF for nonlinear systems is required. Two most common approaches are to use either the Extended Kalman Filter (EKF) or Unscented Kalman Filter (UKF). The performance of these two algorithms is compared for example in [28] and

[29] for localization based on angle data and in [30] and [31] for localization based on RSSI. The EKF works by computing a Jacobian of the nonlinear function and therefore linearizing the nonlinear model about a working point. Despite its widespread use, the EKF falls short while used for systems that are highly nonlinear and requires computation of the Jacobian matrix for its implementation. The UKF, described in [32], uses an unscented transform which approximates the Gaussian distribution by choosing a set of sigma points and by applying the nonlinear function to each point. This yields a cloud of transformed points which is used for calculation of the new statistics. Both the EKF and UKF have been implemented for the localization system and compared in simulations with generated sensor data. Based on the experimental comparison, in which the UKF performed slightly better the UKF was chosen as the estimation algorithm used for the localization. The UKF implementation is in detail described in [33].

Although all MAVs in the formation measure their respective radiation patterns approximately at the same moment, the UKF used in this localization algorithm processes the received data sequentially and uses only measurements from one MAV in each filter step. This method can be used because the localized beacon is static and the measurements are time-independent. This approach was chosen in order to maximize the number of measurements used in localization. The filter contains a validation gate which detects bad measurements and discards the whole update step in case of detection. If measurements from multiple MAVs were used in each step, the filter would have to either reject all of them or use some additional method to detect which specific measurement was the faulty one.

During simulations, it was discovered that if the initial position estimate is on the other side of the first MAV than the real beacon, the distance estimation from RSSI can cause the filter to diverge and therefore decreases its performance because it takes time for the UKF to converge again. Therefore, the filter uses only AoA data in the steps performed in the first position of the MAV formation trajectory in order to establish a beacon position estimate in the correct direction from the formation. The AoA-only estimation is achieved by setting the standard deviation of RSSI in the $\mathbf{R}$ matrix to a very large value as written in Section 4.4.4.

If the algorithm localizes more beacons at the same time, a separate instance of UKF is created for every beacon.

4.4.1 Weights and sigma points calculation

The sigma points, used by the unscented transform, are calculated using Van der Merwe's scaled sigma point algorithm. The calculation of sigma points is controlled by three parameters α, β and κ, which control the distance of the individual sigma points from their mean. The points are calculated from the input μ as

$$\vec{\chi}_0 = \vec{\mu}, \tag{4.4}$$

$$\vec{\chi}_i = \begin{cases} \vec{\mu} + [\sqrt{(n+\lambda)\mathbf{P}}]_i & i \in [1, \ldots, n] \\ \vec{\mu} - [\sqrt{(n+\lambda)\mathbf{P}}]_{i-n} & i \in [n+1, \ldots, 2n], \end{cases} \tag{4.5}$$

$$\lambda = \alpha^2(n+\kappa) - n, \tag{4.6}$$

where i index denotes the sigma point number and chooses the i-th column vector of the matrix, n is the dimension of the state vector, and $\mathbf{P}$ is the state covariance matrix. The first sigma point is the mean of the input and the rest of the sigma points is chosen symmetrically around the mean. Cholesky decomposition is used to calculate square root of the matrix. Next, the weights used for calculation of means and covariances from sigma points are computed as

$$W_0^m = \frac{\lambda}{n+\lambda}, \tag{4.7}$$

$$W_0^c = \frac{\lambda}{n+\lambda} + 1 - \alpha^2 + \beta, \tag{4.8}$$

$$W_i^m = W_i^c = \frac{1}{2(n+\lambda)}, \; i \in [1, \ldots, 2n], \tag{4.9}$$

where W_i^m are weights for means and W_i^c are weights for covariances. The values of the parameters have been chosen as

$$\alpha = 0.001,$$

$$n = 2,$$

$$\kappa = 3 - n,$$

$$\text{and } \beta = 2$$

4.4.2 Predict step

During the predict step, the sigma points are passed through the system model and therefore projected forward in time as

$$\boldsymbol{\mathcal{Y}} = \mathbf{A}\boldsymbol{\chi} \tag{4.10}$$

where $\boldsymbol{\mathcal{Y}}$ are sigma points in step $k+1$, $\boldsymbol{\chi}$ are sigma points in step k and $\mathbf{A}$ is the system model which, in our case, is just an identity matrix. Afterwards a new state estimate $\bar{\vec{x}}$ and covariance $\bar{\mathbf{P}}$ are calculated as

$$\bar{\vec{x}} = \sum_{i=0}^{2n} W_i^m \vec{\mathcal{Y}}_i, \tag{4.11}$$

$$\bar{\mathbf{P}} = \sum_{i=0}^{2n} W_i^c (\vec{\mathcal{Y}}_i - \bar{\vec{x}})(\vec{\mathcal{Y}}_i - \bar{\vec{x}})^T + \mathbf{Q} \tag{4.12}$$

where W_i^m and W_i^c denote the i-th element in the respective weight vector calculated in Section 4.4.1, $\vec{\mathcal{Y}}_i$ chooses the i-th vector of the $\boldsymbol{\mathcal{Y}}$ matrix and $\mathbf{Q}$ denotes the state process covariance matrix whose values are described in Section 4.4.4.

4.4.3 Update step

During the update step the sigma points are converted into the measurement space by passing them through the nonlinear measurement function defined in Section 3.1. The mean and covariance of the measurement sigma points are computed using the unscented transform:

$$\boldsymbol{\mathcal{Z}} = h(\boldsymbol{\mathcal{Y}}), \tag{4.13}$$

$$\vec{\mu}_z = \sum_{i=0}^{2n} w_i^m \vec{\mathcal{Z}}_i, \tag{4.14}$$

$$\mathbf{P_z} = \sum_{i=0}^{2n} w_i^c (\vec{\mathcal{Z}}_i - \vec{\mu}_z)(\vec{\mathcal{Z}}_i - \vec{\mu}_z)^T + \mathbf{R}. \tag{4.15}$$

The residual $\vec{y}$ of the measurement and the computed mean is calculated as

$$\vec{y} = \vec{z} - \vec{\mu}_z. \tag{4.16}$$

After subtraction of the two vectors, the angle element is normalized to interval $(-\pi, \pi)$. This applies to equations (4.16) and (4.18).

In order to detect and reject bad measurements, a validation gate is used. The topic of validation gating is described in [34] in detail. It works by rejecting the measurements which are too distant from the current state of the filter. This way the robustness of the UKF is greatly improved. The validation gate is set up by calculating the Normalized estimation error squared (NEES) e_z^2 as

$$e_z^2 = \vec{y}^T \mathbf{P_z}^{-1} \vec{y}. \tag{4.17}$$

e_z^2 is a scalar value with a Chi-squared distribution with r degrees of freedom, where r is the dimension of the measurement vector $\vec{z}$. If e_z^2 is outside the desired bounding values, the measurement is rejected. The used gate is set to discard measurements which satisfy

$$e_z^2 > 4 \cdot q_{\chi^2}(0.95, 2),$$

where $q_{\chi^2}(p, n)$ is a quantile of Chi-squared distribution for confidence level p and n degrees of freedom. The value of $4 \cdot q_{\chi^2}(0.95, 2)$ has been determined from the performance of the filter on real experimental data. When a measurement is discarded the UKF performs only its predict step which in this case means a change in the state covariance only and no update step is made.

In order to prevent a situation when the state estimate and covariance were too faulty and the validation gate would discard all measurements, the gate is only allowed to reject 3 measurements in a row and furthermore it cannot reject any measurements made in the first 3 steps of the filter.

If the measurement passes through the validation gate the cross covariance of the state and the measurements and the Kalman gain are computed as

$$\mathbf{P_{xz}} = \sum_{i=0}^{2n} W_i^c (\vec{\mathcal{Y}}_i - \vec{\bar{x}})(\vec{\mathcal{Z}}_i - \vec{\bar{\mu}}_z)^T, \tag{4.18}$$

$$\mathbf{K} = \mathbf{P_{xz}} \mathbf{P_z}^{-1}. \tag{4.19}$$

Finally, the new state estimate and the new state covariance are computed as

$$\vec{x} = \vec{\bar{x}} + \mathbf{K}\vec{y}, \tag{4.20}$$

$$\mathbf{P} = \bar{\mathbf{P}} - \mathbf{K}\mathbf{P_z}\mathbf{K}^T. \tag{4.21}$$

4.4.4 Filter parameters

The UKF parameters have been chosen in order to optimize the filter performance on data gained from the real world experiments. The initial state estimate $\vec{x}_0$ is set to be in the center of the MAV formation. In case of 3 MAVs $\vec{x}_0$ is obtained as

$$\vec{x}_0 = \begin{bmatrix} \frac{x_1+x_2+x_3}{3} \\ \frac{y_1+y_2+y_3}{3} \end{bmatrix}, \tag{4.22}$$

where $x_{1\ldots3}$ denote the x coordinate of the respective MAV and $y_{1\ldots3}$ denote the y coordinate of the respective MAV. The initial value of the state covariance

$\mathbf{P}$ matrix has been chosen as

$$\mathbf{P} = \begin{bmatrix} 70 & 0 \\ 0 & 70 \end{bmatrix}$$

to reflect a high uncertainty in the initial state estimate. The process noise $\mathbf{Q}$ matrix has been chosen as a diagonal matrix as

$$\mathbf{Q} = \begin{bmatrix} 0.1957^2 & 0 \\ 0 & 0.1957^2 \end{bmatrix}.$$

The σ_{RSS} parameter which represents the RSSI deviation in the measurement noise $\mathbf{R}$ matrix is set to

$$\sigma_{RSS} = 1000 \text{ dBm}.$$

for the filter steps performed in the first position of the MAV formation trajectory in order to make the UKF use only AoA information in the beginning. For the remaining steps, the parameter has been chosen as

$$\sigma_{RSS} = 7.9 \text{ dBm}.$$

Chapter 5

MAV control

5.1 Radiation pattern measuring by rotating MAV

Another approach to measuring the radiation pattern evaluated in this thesis is rotating the whole MAV along its z axis. This approach requires no rotating device to be attached to the antenna which makes it a more robust option because there are less mechanical parts that can break during use. This approach works by sampling the 360 degree rotation into 65 points and passing a trajectory of these points to the MAV's controller. The controller follows this trajectory in a way that the movement from one point to another takes 0.2 s without exceeding the maximal allowed speed. This means that one radiation pattern sweep should theoretically take

$$t_s = (65 - 1) \cdot 0.2 = 12.8\ s.$$

The value of 65 points per trajectory was chosen as an appropriate value which should allow the MAV to measure a sufficient amount of samples and not spend too much time sweeping one radiation pattern. This approach to sweeping was tested in the Gazebo simulator and then in a real experiment with one MAV, described in Section 7.2, and in the final experiment with active localization, described in Section 7.5. One of the radiation patterns measured in the experiment with one MAV can be seen in Figure 5.1. It contains individual measured samples, preprocessed pattern as described in Section 4.2, the detected AoA and the real AoA.

During the experiments and the simulations, a number of disadvantages of using this approach as opposed to the use of a rotating antenna were

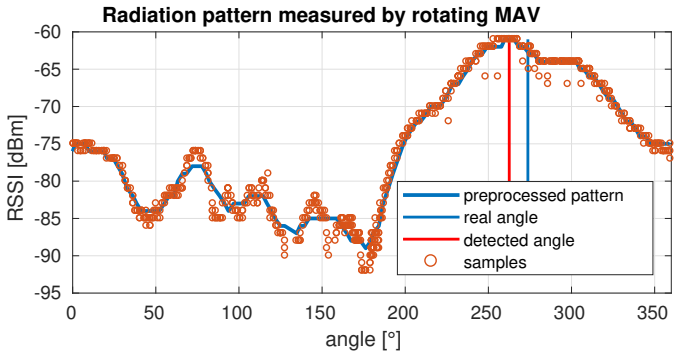

Figure 5.1: Radiation pattern measured by rotating the whole MAV

discovered. First, the position of the MAV during the rotation is not stable which may reduce the localization accuracy. This fact can be overcome by using a lower rotation speed but longer time per one sweep means a lower total number of measurements that can be done during one MAV flight. Second, the use of rotating antenna is more robust in situations when the frequency of measured samples is not constant. The rotating antenna can stop in each rotational position and wait for a sufficient number of samples. Because of these reasons, the rotating antenna approach was used as the main method of radiation pattern measurement for all further experiments described in this thesis but rotating MAV approach still remains a viable option which can be used when no rotating device is available.

5.2 Formation control

During the localization process, the MAV formation needs to actively react to current position estimates and reposition itself to achieve the best possible localization results. The formation control algorithm was implemented for a group of 3 MAVs but could be easily modified for the use of a different number of drones.

The formation has got the shape of an equilateral triangle with the MAVs located in its vertices. The vertices lie on a circumscribed circle with radius r equal to the distance of the vertices from the center of the triangle. All MAVs fly in the same altitude. The location, rotation, and size of the formation is determined by the following parameters: C_x and C_y which denote coordinates of the center of the triangle, radius r and angle θ which is defined as the angle between the positive half of x axis and the line between the first MAV and the center of the triangle. The shape of the formation with all its parameters is shown in Figure 5.2b.

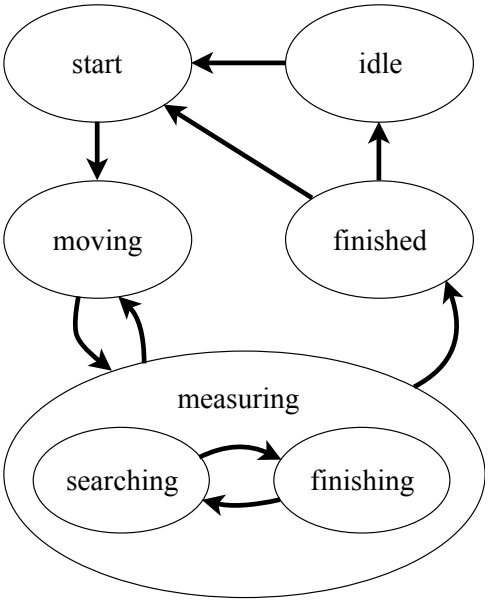

(a) : Diagram of state machine used to control the formation

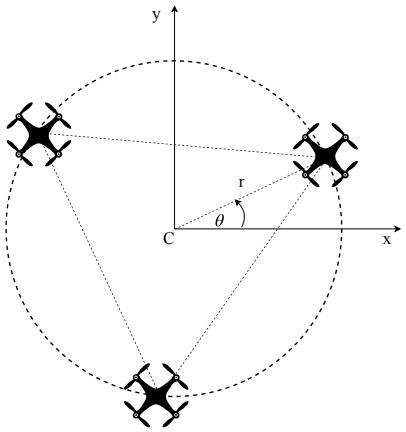

(b) : Formation parameters[1]

Figure 5.2: Formation control and its parameters

The controller itself contains a state machine consisting of 5 states: *start*, *idle*, *moving*, *measuring* and *finished*. The *measuring* state contains 2 substates: *searching* and *measuring*. The state machine is depicted in Figure 5.2a. If there are multiple beacons the formation localizes only one at a time and starts the localization of the next beacon after the position of the previous one is found.

The state machine is initialized in the *idle* state where it waits for a call to start localization. When the localization starts it transfers to the *moving* state and the formation forms itself with its center calculated as the center of the triangle formed by current positions of the MAVs.

After all MAVs reach their appropriate destinations the state machine transfers to the *measuring* state and the *searching* substate. In this state, all MAVs measure their radiation patterns and pass the obtained data to the UKF. After a new estimate of the localized beacon's position is produced, the controller transfers back to the *moving* state with a target position of the new estimate being at the center of the formation.

The formation continuously improves its estimation of the beacon's position and repositions itself to the place of the new estimate (using the MPC

[1]Drone icon by Leonardo Schneider from the Noun Project

controller described in [23]) until the new estimated position is less than 1 meter away from the last estimate and at least 3 formation measurements have been performed. Then the *measuring* state transfers to the $finishing$ substate. The formation drops to a lower altitude and performs the same measurement-move cycle but rotates itself by $\frac{\pi}{6}$ in every *movement* step. After 4 $finishing$ steps the localization is finished (during the $finishing$ stage, 12 different MAV positions around the beacon are used to gradually improve the beacon position estimate), the last estimated position is returned as the beacon's position and the state machine to the $finished$ state.

If there are any beacons left to localize, the state machine transfers to the *start* state, the *measuring* state transfers back to the *searching* substate and the localization continues with the next beacon. Otherwise, the state machine transfers to the *idle* state.

From the simulations and the data measured in real experiments, $r = 6$ m was empirically chosen as the radius of the formation and the altitudes of 4 m in the *searching* substate and 3 m in the $finishing$ substate were chosen as the appropriate values. The choice of these parameters depends on the scale of the area were a beacon is being localized and the parameters of the used devices.

Chapter 6

Simulations

Before full deployment of the implemented algorithm to real hardware and performing real outdoor experiments, the Gazebo simulator was used to verify the system functionalities and correct performance of the implementation. ROS nodes were implemented in order to simulate the measurement of RSSI values for different positions of the MAVs and different rotations of the antenna.

The simulation uses one of the radiation patterns measured in the preliminary experiment described in Section 7.1 as a source dataset on which all the simulated measurements were based. The measured radiation pattern was smoothed using moving mean, and cubic spline interpolation was used to calculate more detailed samples. During the simulation, the source values are shifted in angle according to the current rotation of the antenna, current yaw of the MAV, and the bearing between the MAV and the localized beacon. Furthermore, the RSSI values are scaled with distance according to equation (3.7) using parameters identified from experiments described in Section 7.1, 7.2 and 7.3. Random values from a normal distribution are used to model the noise influencing the RSSI measurements and the inaccuracy in AoA estimation.

The simulation offers a basic verification of the implemented algorithm functionalities before using it on real hardware. However, a lot of other influences which this simulation does not support, occur under real-world conditions. For example, the shape of the simulated radiation pattern stays approximately the same and therefore the estimation of angle uncertainty described in Section 4.3 has got a low effect on localization performance.

Furthermore, the AoA estimation error is greater with a bigger vertical angle between the antenna and the localized beacon. Simulation of these influences could be a part of future work on this subject since these phenomena have been observed during the final experiments shortly before the thesis deadline. Earlier experimental evaluation in the full scope was not possible due to weather conditions. Nevertheless, the real-world experimental evaluation presented sufficient performance.

6.1 Simulation of active localization

A simulation of active localization of 2 beacons by a formation of 3 MAVs was performed in order to verify the functionality of formation control algorithm described in Section 5.2 and localization algorithm described in Chapter 4. The beacons were placed at zero altitude at positions x: -10, y: -10 and x: 5, y: 15. The noise and error values were drawn from normal distributions

$$e_{RSSavg} \sim \mathcal{N}(0, 4),$$

$$e_{RSS} \sim \mathcal{N}(0, 2),$$

$$e_{\theta} \sim \mathcal{N}(0, 30^{\circ}),$$

where e_{RSSavg} is the deviation of average RSSI of the radiation pattern from the theoretical curve, e_{RSS} is the random noise added to every measured RSSI value and e_{θ} is the error of AoA estimation in degrees. The MAV formation started with its center at x: 6.17 m and y: -0.31 m and gradually localized both beacons. Figure 6.1a shows an example of a measured radiation pattern from this simulation along with the real angle where the beacon is located and the AoA detected by the localization algorithm. Figure 6.1b depicts the localization error calculated as the Euclidean distance between current estimate and real beacon position for both beacons. Beacon 1 was localized in 27 steps (9 moves of the formation) and beacon 2 was localized in 36 steps (12 moves of the formation). The final localization error of the first beacon is 2.38 m and the final estimation error of the second beacon is 1.77 m.

Figure 6.2a contains positions of the MAVs, beacon and progression of the estimated position during the localization of beacon 1. MAV positions belonging to the same step are connected by a dashed line. Figure 6.2b shows the same but displays the progression during the localization of beacon 2. Figure 6.3 contains screenshots from the video of the simulation, recorded in the Gazebo simulator itself, from two different steps of the searching phase of beacon 1 localization. The individual MAVs are highlighted by the black circles surrounding them and the beacons are highlighted by the red circles.

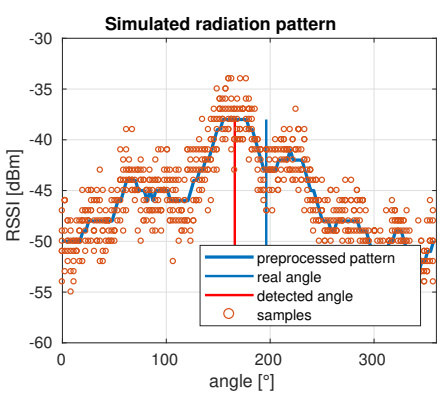

(a) : Example of a simulated radiation pattern

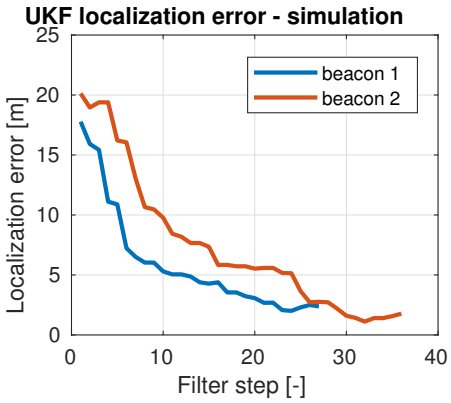

(b) : UKF localization error for 2 beacons

Figure 6.1: Simulated radiation pattern and localization error

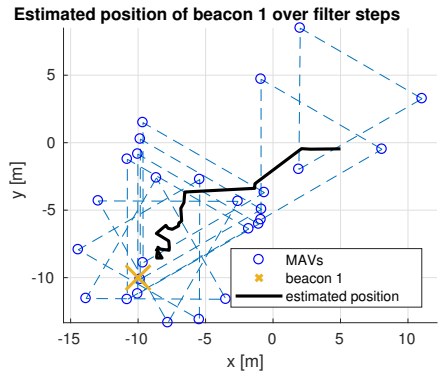

(a) : Position estimation of beacon 1

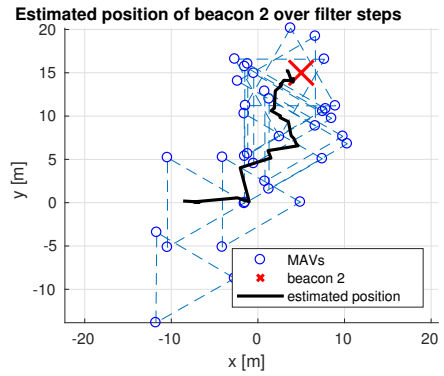

(b) : Position estimation of beacon 2

Figure 6.2: Estimated positions of each beacon over filter steps along with the positions of the MAVs

Figure 6.4 contains screenshots from 2 steps of the finishing phase of beacon one localization. Finally, Figure 6.5 contains 2 pictures from the localization of beacon 2.

A video of the simulation can be seen on youtube.[1] Active localization verified in this simulation was later tested in a real-world experiment with a formation of three MAVs and one beacon, as described in Section 7.5.

[1] `https://youtu.be/GB01JsNOv0w`

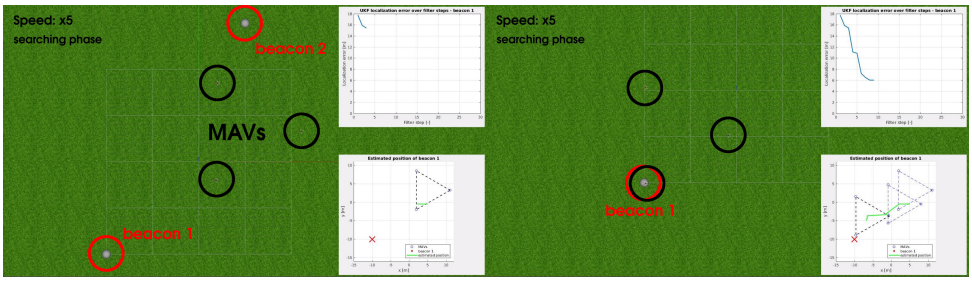

(a) : Second formation position during beacon 1 localization

(b) : Formation position number 4 during beacon 1 localization

Figure 6.3: Gazebo - localization of beacon 1 during searching phase

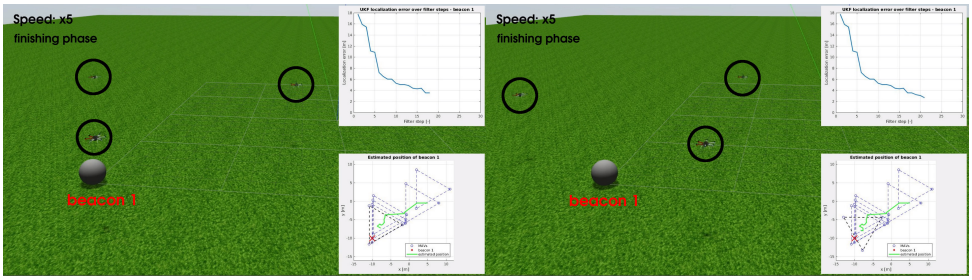

(a) : First finishing step

(b) : Second finishing step

Figure 6.4: Gazebo - localization of beacon 1 during finishing phase

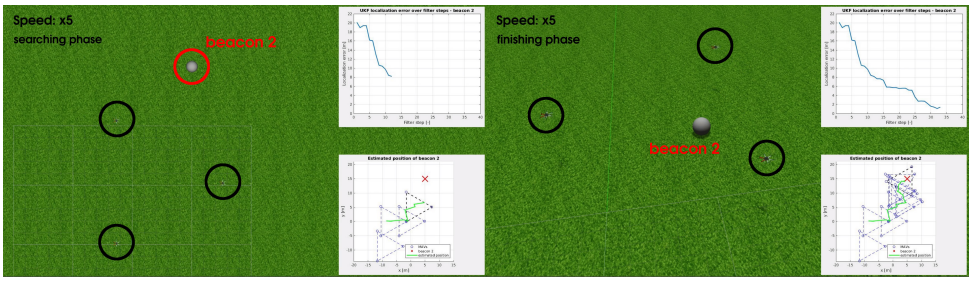

(a) : Localization of beacon 2 - searching phase

(b) : Localization of beacon 2 - finishing phase

Figure 6.5: Gazebo - localization of beacon 2

Chapter 7

Real experiments

Five different real-world experiments are described in this chapter. In Section 7.1, identification of the path loss parameters P_0 and γ is described. Section 7.2 contains an experiment with one drone emulating a moving MAV formation. Section 7.3 shows an experiment with localization using a single MAV following a rectangular trajectory. An experiment with a formation of three MAVs following predefined trajectories is described in Section 7.4. The final experiment, where the active localization algorithm along with the rotating MAV approach was verified, is described in Section 7.5. A summary of the experimental results and a comparison with the previous works are written in Section 7.6.

7.1 Dependency of average RSSI on distance

For the purpose of localization algorithm design, the parameters P_0 and γ from equation (3.7) needed to be identified. In order to achieve this, a measurement using a beacon and one MAV was performed. This experiment was carried out on an empty field in order to eliminate the effect of shadowing and minimize multipath effects interfering with the RSSI values. The beacon was placed on the ground at zero altitude and the MAV gradually flew away from the beacon in a straight line while measuring the current radiation pattern in multiple points along its trajectory.

This measurement was performed at 3 different altitudes. First, the MAV

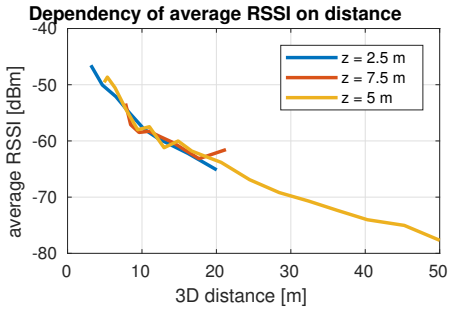

(a) : Dependency of average RSSI values on 3D distance for various altitudes

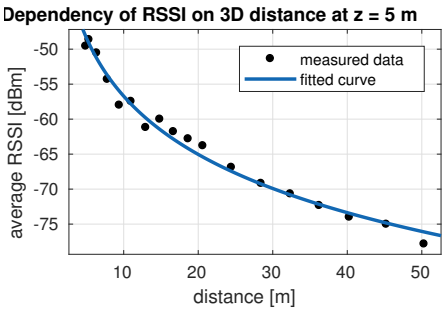

(b) : Average RSSI values measured at z = 5 m with fitted curve

Figure 7.1: Dependency of average RSSI values on the distance between MAV and beacon measured in experiment 7.1

flew in the altitude of 5 m and in 2D distance from 0 up to 50 m away from the beacon. 18 different radiation patterns were measured along this trajectory. During the second measurement, the MAV moved from 2 to 20 m away in the altitude of 2.5 m while doing a measurement in 8 points and next the MAV repeated the same 8 point measurement in the altitude of 7.5 m. A short video from this experiment can be seen on youtube.[1]

An average RSSI was calculated for every radiation pattern measured as described in Section 4.2. The dependency of this average RSSI on the 3D distance between the beacon and the MAV is plotted in Figure 7.1a. It can be seen that the dependency is comparable for all 3 altitudes although it contains more noise in shorter distances due to multipath effects. The Equation (3.7) was fitted to the data measured from the 5 m altitude using a least squares method. This way the parameters were identified as

$$P_0 = -29.06, \ \gamma = 2.765.$$

Figure 7.1b shows the measured data along with the fitted curve.

Furthermore, by calculating the deviation of the angle with maximal RSSI from the real AoA it was discovered that the deviation is larger in a closer distance and in higher altitudes. This is probably caused by a bigger vertical angle between the antenna and the beacon which increases as the distance get smaller and as the MAV altitude grows. This highlights the advantage of using a larger formation moving at a lower altitude during the localization and the need for reactive position and altitude changing.

[1] `https://youtu.be/lpT_dYN07Gg`

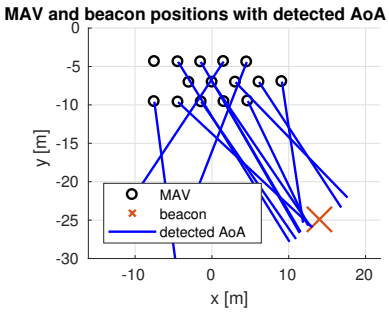

(a) : x-y plot of MAV and beacon positions along with detected AoA

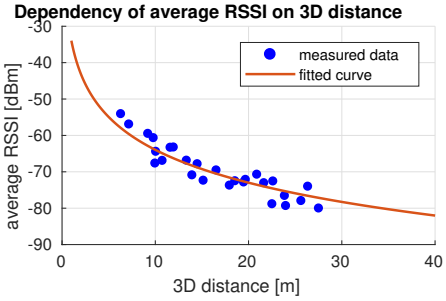

(b) : Average RSSI measured in 2 urban experiments along with fitted curve

Figure 7.2: Data measured from experiments with one MAV

7.2 One MAV emulating a moving formation

This experiment was meant to emulate a few moves of the whole formation using one MAV. The MAV made measurements in 15 predefined points emulating 5 moves of a 3 drone formation. The individual positions of the MAV along with lines representing the detected AoA and the beacon position can be seen in Figure 7.2a. The correlation coefficient of calculated σ_θ values and AoA estimation error (as defined in Section 4.3) is 0.713 at statistical significance 0.0028.

During this experiment, it became clear that the frequency of samples received by the antenna is too variable to be able to reliably receive enough samples per each position when a constant time is spent in each position, and sometimes no transmission is realized. For example, during two of these measurements, no samples were received due to XBees being unable to establish communication. These are the leftmost points in the upper and middle row in Figure 7.2a where no AoA is plotted. After this experiment, a waiting period for a constant number of samples in each position and a timeout after a certain time threshold is exceed were implemented in the algorithm as described in Section 4.1.

This experiment was performed on a large empty outdoor urban area. It was discovered that the RSSI path loss parameters differ from the parameters identified in Section 7.1. This can be caused by bigger radio interference in the urban environment. To account for this, new parameters were identified from data measured in this experiment and in the experiment described in Section 7.3. The data were measured only in distances shorter than 28 m from the beacon, therefore the path loss exponent γ was set to have an upper limit of 3 because it is assumed that the RSSI falls more slowly with larger

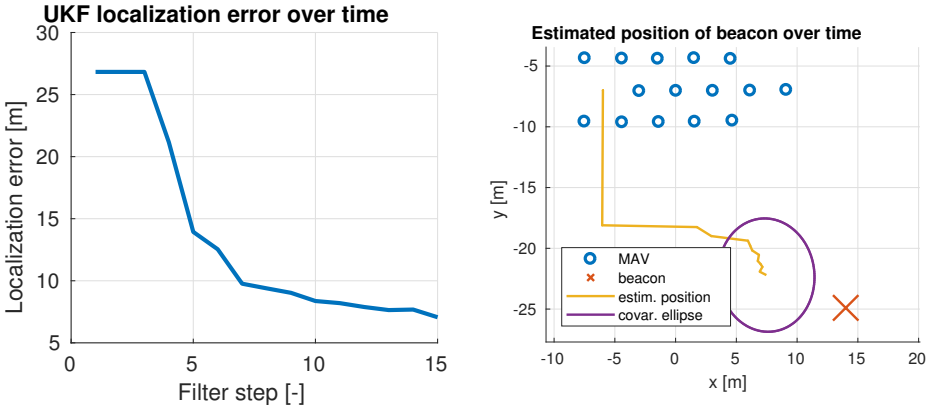

(a) : UKF localization error over filter steps

(b) : Estimated beacon position over filter steps

Figure 7.3: Positions estimated by the UKF during the experiment with one MAV emulating a moving formation

distances. The new parameters were thereafter identified as

$$P_0 = -33.96, \ \gamma = 3.$$

The root mean square error (RMSE) of average RSSI values measured in this experiment from the fitted curve is 2.53 dBm.

The measured data were passed to the UKF in a way emulating that a formation of 3 MAVs made the measurements. Figure 7.3a shows the progression of UKF localization error over the number of executed filter steps. The error e_{ukf} is calculated as

$$e_{ukf} = \sqrt{(x_{est} - x_B)^2 + (y_{est} - y_B)^2}, \tag{7.1}$$

where x_{est} and y_{est} are the current estimates of beacon coordinates and x_B and y_B are the real beacon coordinates. The final error is 7.06 m and the filter keeps converging to the correct position which suggests that with more measurements, which would be available with a full formation, the beacon should be successfully localized. Figure 7.3b depicts the progression of the estimated beacon position in the x-y plane along with the beacon and the individual MAV positions. A covariance ellipse of the final estimate which shows the 95% confidence area is plotted. It can be seen that the beacon is still outside this area which highlights the necessity of using more measurements and adaptive formation control.

The rotating MAV approach described in Section 5.1 was also verified during this experiment. The MAV made 5 measurements at the same positions as the bottom row in Figure 7.2a. The approach was proved to work but the disadvantages described in Section 5.1 were discovered.

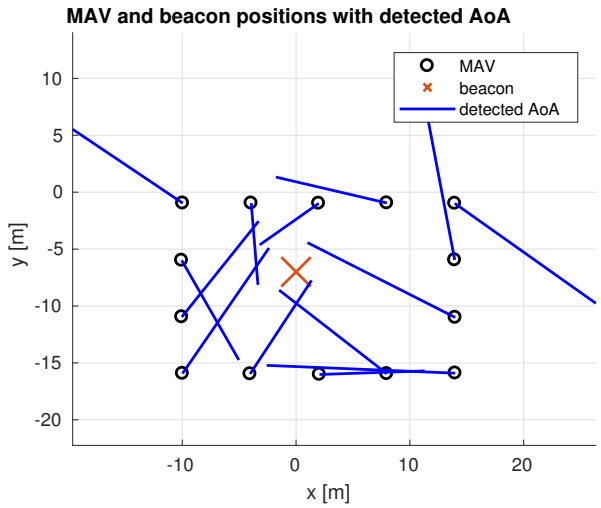

Figure 7.4: MAV positions with detected AoA - experiment with a single MAV following a rectangular trajectory

7.3 One MAV following a rectangular trajectory

This experiment was performed in the same workspace as the experiment described in Section 7.2. One MAV was following a rectangular trajectory around the beacon and during this time it made 14 different measurements. The same path loss parameters and the same UKF parameters as in the previous experiment were used. The first MAV position was chosen as the initial estimate of beacon position. The positions where the MAV made its measurements along with the detected AoA can be seen in Figure 7.4. The beacon was placed at x: 0, y: -7. The MAV started at the lower left corner of the rectangle and then followed the trajectory in a counter-clockwise direction.

The RMSE of average RSSI values from the theoretical fitted curve is 2.6 dBm. The correlation coefficient of σ_{theta} and AoA estimation error is 0.80 at statistical significance 0.0005. Figure 7.5a shows the progression of UKF localization error over the number of performed filter steps. It can be seen that the error dropped from 13.39 m to 4.22 m in just 5 filter steps but then stayed roughly the same for the rest of the localization. The final localization error is 3.88 m. Figure 7.5b contains the progression of estimated beacon position in xy plane along with covariance ellipse of the final estimate. It can be seen that the beacon position lies inside this 95% confidence area.

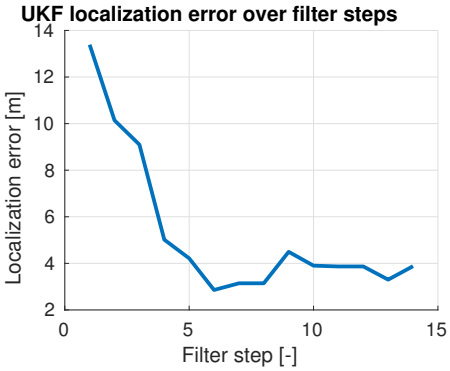

(a) : UKF localization error over filter steps

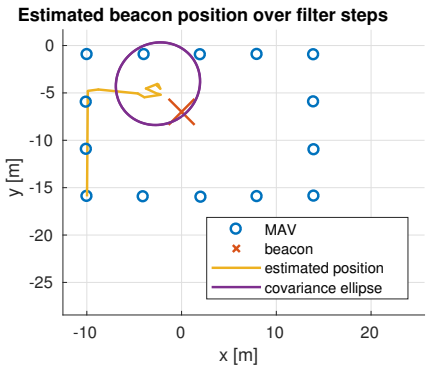

(b) : Estimated beacon position over filter steps

Figure 7.5: Positions estimated by the UKF - experiment with a single MAV following a rectangular trajectory

7.4 MAV Formation sweeping a large area

This experiment was performed in the same place as Experiment 7.1, therefore the UKF uses the path loss parameters identified during that experiment. A formation of 3 MAVs and one beacon were used during this experiment. The formation swept a 65 by 50 m large area by traveling to 16 predefined positions resulting in 48 different radiation pattern measurements. The predefined trajectory can be seen in Figure 7.6. The formation starts in the lower left corner. During the first flight described in Subsection 7.4.1 the MAVs made 23 individual measurements and the experiment was stopped due to technical difficulties but the measured data can still be used for partial localization. During the second flight described in Subsection 7.4.2 the MAVs made all 48 individual measurements. A video of the second flight can be seen on youtube. [2]. Figure 7.10 contains a picture from the video depicting measurement of the individual radiation patterns. Figure 7.11 contains another picture from the video which shows the MAV formation following the predefined trajectory and localizing the beacon.

7.4.1 First flight

Figure 7.7a shows the MAV positions during this experiment along with the detected AoAs which are depicted by lines pointing from the appropriate MAV positions. Data from all 3 MAVs in formation are available only from the first

[2] `https://youtu.be/3fBW5CertHk`

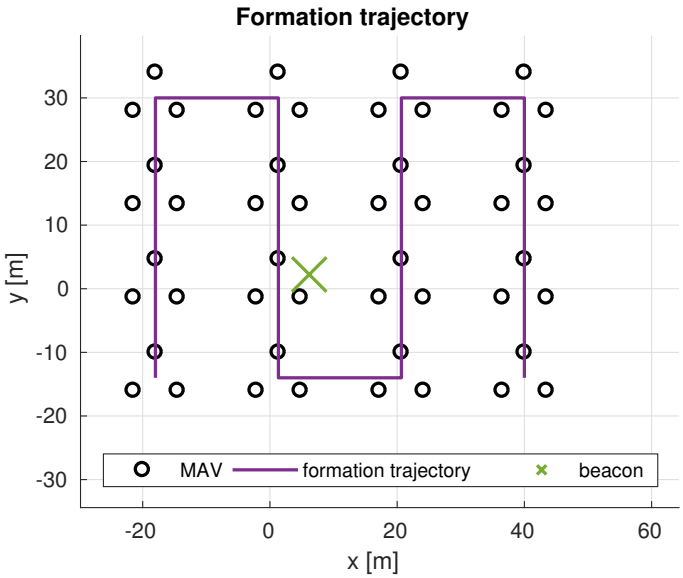

Figure 7.6: Predefined formation trajectory - experiment with an MAV formation sweeping a large area

3 formation positions. In the rest of the positions, only data from 2 MAVs were obtained. The correlation of estimated AoA uncertainty σ_θ and AoA estimation error is 0.28 at 0.19 statistical significance which is significantly lower than in the previous experiments but a correlation still exists. The RMSE of average RSSI values from the theoretical curve is 3.9 dBm.

Figure 7.7b contains the progression of UKF localization error over the number of performed filter steps. It can be seen that using the measured data the localization error dropped by approximately 20 m during the filter run. The final localization error is 9.8 m.

7.4.2 Second flight

During the second flight, the MAVs made a total number of 48 different measurements. The positions were the measurements were performed along with the detected AoAs can be seen in Figure 7.8a. The correlation of σ_θ and AoA estimation error is 0.29 at 0.043 statistical significance. The average RSSI values along with the theoretical curve are shown in Figure 7.8b. The RMSE of the values from the theoretical curve is 3.45 dBm.

During this experiment, the largest number of correct measurements was

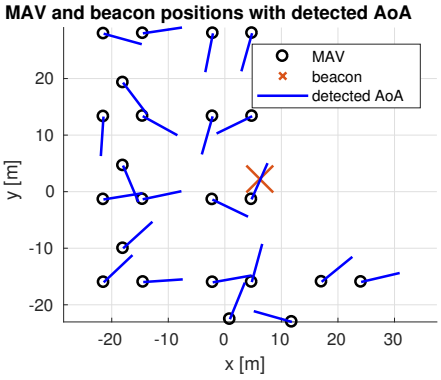

(a) : x-y plot of MAV and beacon positions along with detected AoA

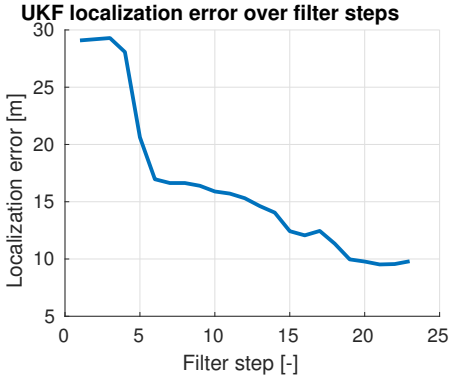

(b) : UKF localization error

Figure 7.7: MAV positions with detected AoA and UKF localization error from first flight of formation with predefined trajectories

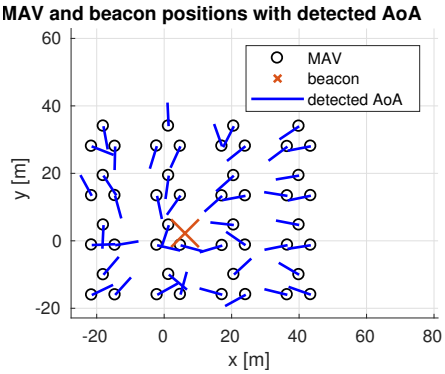

(a) : x-y plot of MAV and beacon positions along with detected AoA from experiment with a formation following predefined trajectories

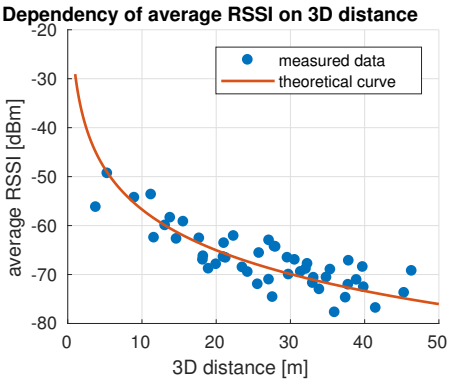

(b) : Dependency of average RSSI on distance from formation experiment

Figure 7.8: Measured data from the second flight of MAV formation

collected therefore the data from this experiment were used for tuning the parameters of the UKF with the goal of minimizing the final localization error and the performance of the filter with these parameters was then verified on data gained from the other experiments. The UKF parameters are described in Section 4.4.4.

Figure 7.9a shows the progression of UKF localization error over the number of performed filter steps for 3 different settings of the filter. The $RSSI + AoA$ setting uses the filter parameters described in Section 4.4.4. It can be seen that its localization error drops to 1.66 m in 25 filter steps end then keeps slowly converging to the real beacon position. The final localization error is 0.04 m. The AoA setting uses just the AoA data for localization which was

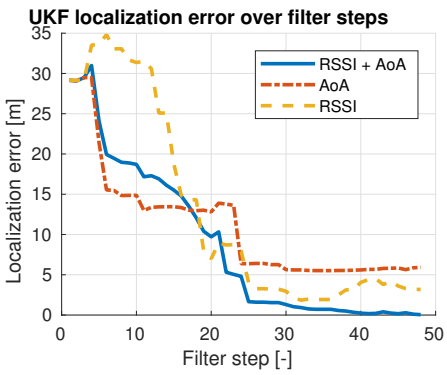

(a) : UKF localization error for different filters

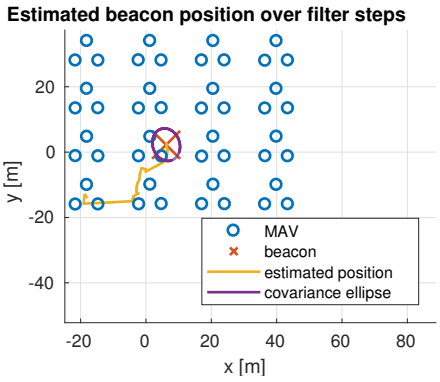

(b) : Estimated beacon position over filter steps

Figure 7.9: Localization results from the second flight of MAV formation

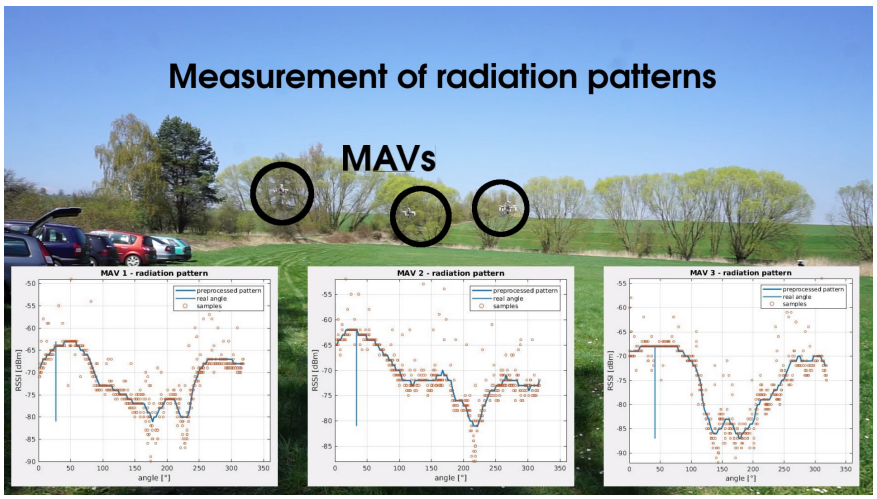

Figure 7.10: Measurement of radiation patterns during the second flight in the experiment with MAV formation following a predefined trajectory

done by setting the σ_{RSS} parameter to a very large value (1000 dBm) and tuning the $\mathbf{Q}$ matrix for the best possible localization results. In this case, the final localization error is 5.92 m. The $RSSI$ setting uses only the RSSI data which is set by multiplying the σ_θ parameters by a large scalar value (1000) and tuning the $\mathbf{Q}$ matrix and σ_{RSS} parameter to produce a good and stable filter performance. The performance is again worse than the performance of the hybrid $RSSI + AoA$ filter and the final localization error is 3.19 m.

Figure 7.9b depicts the progression of the $RSSI + AoA$ UKF estimated position in the xy plane. It can be seen that the estimate starts with its initial value in the first formation position and then gradually converges to the real beacon position. A covariance ellipse of the final estimate representing the 95% confidence area is plotted as well.

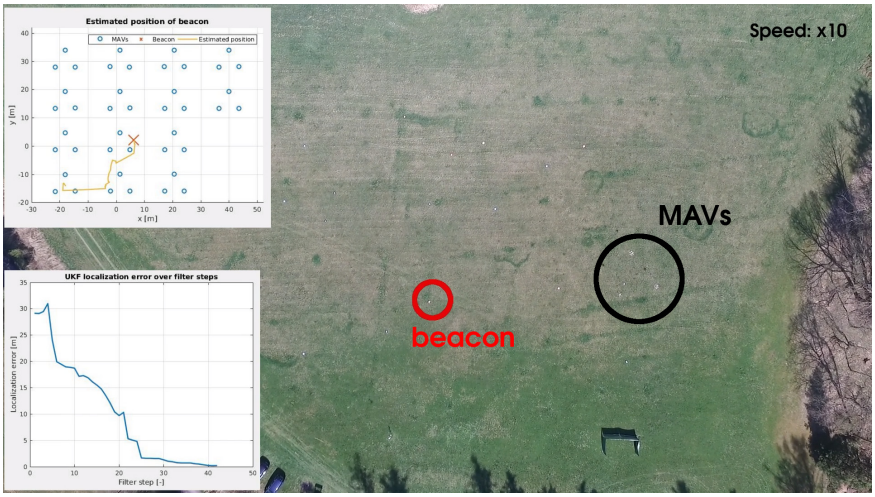

Figure 7.11: Localization of the beacon during the second flight in the experiment with MAV formation following a predefined trajectory

7.5 Active localization

During this experiment, functionalities of the beacon position estimation along with the formation control algorithm, described in Section 5.2, were verified. This experiment was performed in the same workspace as experiments described in Sections 7.2 and 7.3, therefore the path loss parameters P_0 and γ identified during these experiments were used. During this experiment, a formation of three MAVs was actively localizing one static beacon. The beacon was placed at $x = -2\ m$ and $y = -4.8\ m$ and the MAV formation started with its center in $x = 4.58\ m$ and $y = -21.53\ m$. One of the used MAVs made its radiation pattern measurements using the rotating MAV approach described in Section 5.1. The other two MAVs rotated their antennas using step motors. The MAVs made a total number of 23 individual measurements. The algorithm did not fully complete its *finishing* phase because one of the MAVs failed to submit its estimated position to the UKF which resulted in stopping the localization. This unwanted behavior was fixed after the experimental data were processed. However, the obtained data proved sufficient for beacon localization.

Figure 7.13 contains the MAV positions along with the detected AoAs, where measurements were made. The MAV positions belonging to the same formation position are connected by dashed lines. The RMSE of detected AoA from the real MAV-beacon bearing was 0.61 rad. The correlation coefficient of estimated σ_θ values and the error of AoA estimation was 0.57 at statistical significance 0.00042. Figure 7.12a shows the dependency of average RSSI values of the individual measurements on the 3D distance between MAV and

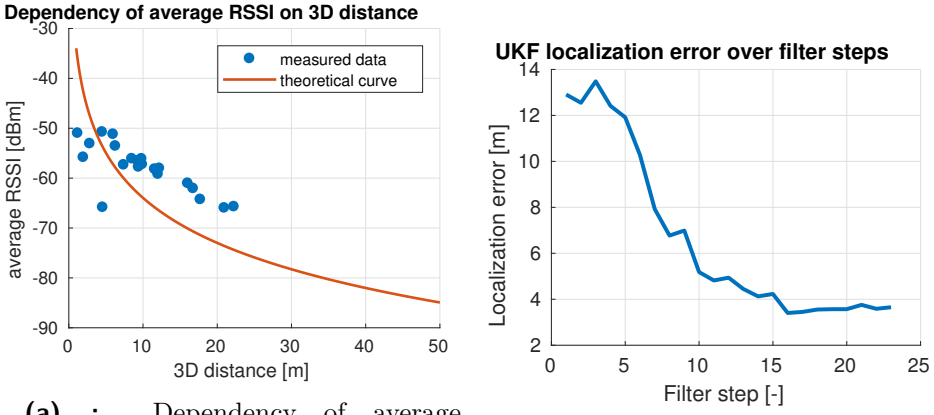

(a) : Dependency of average RSSI values on distance from active localization experiment

(b) : UKF localization error

Figure 7.12: Dependency of average RSSI values on distance and UKF localization error from active localization experiment

beacon. The RMSE of the measured RSSI values was 7.95 dBm. It can be seen that the algorithm performance could be further improved by better calibration of path loss parameters.

The dependency of UKF localization error on the number of performed filter steps can be seen in Figure 7.12b. The final localization error was 3.65 m after 23 filter steps but the UKF has already converged to an error of 3.40 m in step 16 and stayed roughly the same after. Figure 7.14 contains positions of the MAV formation and beacon along with the development of the estimated position over the number of filter steps. A covariance ellipse of the final estimate, representing the 95% confidence area, is also plotted.

A video of this experiment can be seen on youtube.[3] The initial MAV and beacon positions can be seen in Figure 7.15, containing a snapshot from the video. Figure 7.16 shows the localization during its finishing phase and Figure 7.17 shows the situation in the finishing phase, after the formation has rotated. In this experiment, the rotating MAV approach proved to be a reliable alternative to rotating the directional antenna using a step motor, e.g. in case of step motor failure. Furthermore, the functionality of the active localization algorithm was verified under real-world conditions. The performance of the algorithm could be further improved by more precise calibration of path loss parameters.

[3] `https://youtu.be/uH3hmT4Aubk`

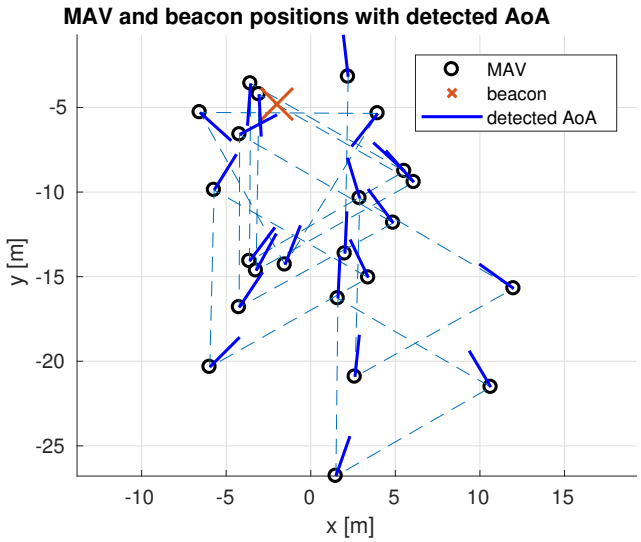

Figure 7.13: MAV and beacon positions along with detected AoA from active localization experiment

7.6 Summary of experiments

The data measured in the aforementioned experiments were used to tune the parameters of the algorithm in order to optimize its performance. Path loss parameters were identified from experiments described in Sections 7.1, 7.2 and 7.3. Parameters of the UKF were tuned based on the performance of the filter on data obtained from the experiment described in Section 7.4.

The experiments have shown that the proposed algorithm performs well under real-world conditions and can be used with a variable number of MAVs. In experiment described in Section 7.2, the final localization error was 7.06 m after 15 filter steps. In the final steps, the UKF kept converging to the correct position, which suggests that with more steps or with the use of the active repositioning, described in Section 5.2, the localization error would improve. In the single drone experiment described in Section 7.3, the final localization error was 3.88 m after 14 filter steps but the UKF already converged to an approximately 4 m error in its fifth step. The experiment from Section 7.4 consisted of two flights of a formation containing 3 MAVs. The localization error in the first flight dropped from 29.08 m to 9.8 m. The data from the second flight were used for tuning the UKF parameters with the goal of minimizing the final localization error. Therefore final localization error was 0.04 m. Furthermore, by using different UKF settings it was shown that the localization algorithm benefits from the fusion of RSSI and AoA data and therefore achieves better results than by using either of these data separately.

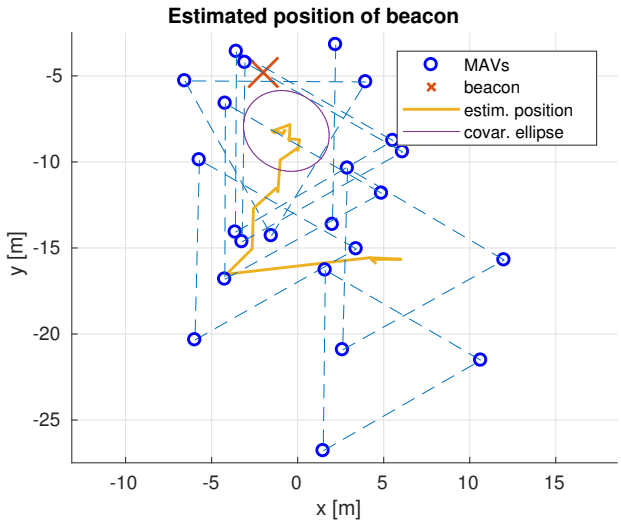

Figure 7.14: MAV and beacon positions along with estimated beacon position from active localization experiment

In the final experiment described in Section 7.5, the functionality of the formation controller, described in Section 5.2, was verified and the rotating MAV approach, described in Section 5.1, was proven to be a viable alternative to the use of a step motor for rotating the antenna. The final localization error during the active localization experiment was 3.65 m which could be further improved by better calibration of the path loss parameters.

This thesis builds upon previous work dealing with localization based on RSSI data obtained from omnidirectional antennas. When compared to results achieved in [1], the estimation using coupled AoA and RSSI measurements, proposed in this work, is more stable than the position estimation from RSSI-only data. Although the RSSI-only approach achieved a lower localization error (under 1.5 m), only indoor experiments in a small room were performed which suggests that outdoor experiments on a larger scale would contain a larger localization error. In [3], an outdoor experiment using Xbee devices with omnidirectional antennas and 2 beacons was performed. In this experiment, the localization error was approximately 4 m for the first beacon and 5 m for the second beacon which is worse than in the experiments with coupled RSSI and AoA measurements where a sufficient number of filter steps was made.

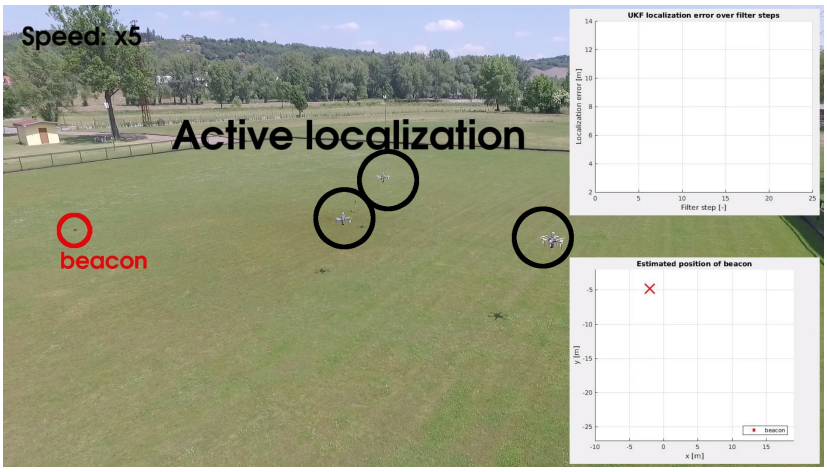

Figure 7.15: Initial MAV positions during the experiment with active localization

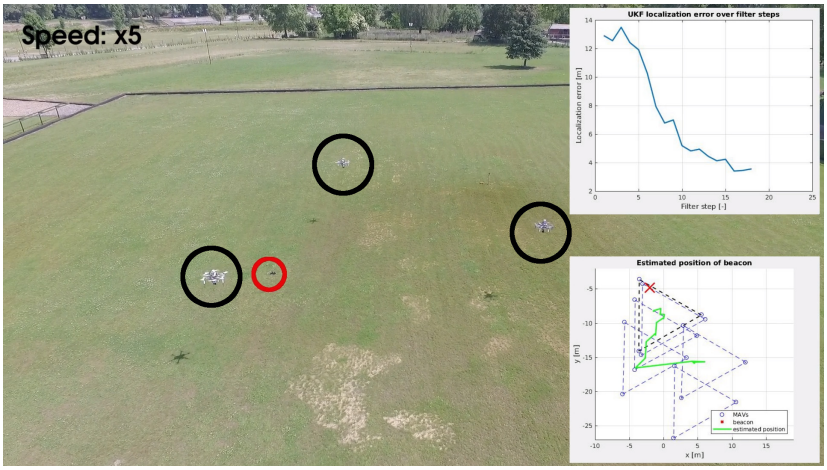

Figure 7.16: Beacon localization in the finishing phase - experiment with active localization

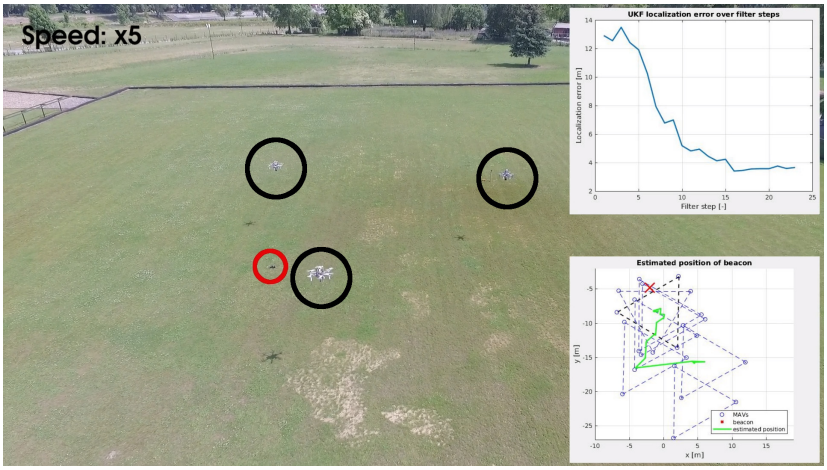

Figure 7.17: Beacon localization in the finishing phase, the formation has rotated - experiment with active localization

Chapter 8

Conclusion

The goal of this thesis was to design a method for localization of sources of RF transmission using a formation of relatively localized MAVs equipped with a rotating directional antenna, implement the method in ROS, experimentally verify in Gazebo simulator and real experiments and compare the achieved results with a system using omnidirectional antennas and with a system using static directional antennas (when the UAV itself is rotating).

Two possible approaches to measuring the radiation pattern of the directional antenna were used - rotating the antenna using a step motor and rotating the whole MAV, as described in Section 5.1. The proposed algorithm, described in Chapter 4, calculates the average RSSI value of each measured radiation pattern and estimates AoA of the transmission along with its uncertainty. A UKF-based approach is used for data fusion and estimation of the RF beacon position. The UKF automatically detects bad measurements and rejects them in order to improve localization performance. The formation controller, described in Section 5.2, takes advantage of the possibility to reactively reshape and reposition the MAV formation in order to quickly and precisely localize the RF beacon.

The proposed algorithm was implemented in ROS and its functionalities were verified in simulations described in Chapter 6. Five different real-world experiments, described in Chapter 7, were performed to verify the system functionalities with real MAV platforms under real-world conditions and test the performance of the proposed approach.

A summary of the achieved experimental results, along with a comparison

with results from previous works achieved with omnidirectional antennas, is written in Section 7.6. The experiments have shown that the proposed approach produces more stable and precise results than the RSSI-only approaches from previous works. A discussion of the use of static directional antennas and rotating whole MAVs is written in Section 5.1. The rotating MAV approach has proven to be a viable alternative to rotating the antennas using step motors but a number of disadvantages were discovered, including less stable MAV position during measurements and low performance in case of variable sample frequency.

It has been shown that the proposed algorithm performs well under real-world conditions. The algorithm benefits from the use of coupled RSSI and AoA measurements and achieves more robust results than either of these methods on their own. The utilization of an actively repositioned MAV formation further improves the localization performance. Furthermore, the possibility to use the rotating MAV approach makes it more practical as it can be used even in situations when an additional rotating device is not available or has suffered a failure.

8.1 Future work

The experimental data measured during the work on this thesis contained a substantial amount of bad measurements. For future work, the use of a directional antenna with higher gain should be considered. With a higher-gain antenna, the AoA estimation would probably be more successful, the UKF would reject fewer measurements and therefore the localization would be faster and more precise. Furthermore, the use of another position estimation algorithm, for example the particle filter, could be considered. According to literature, the particle filter usually outperforms the UKF and many of the related works mentioned in Section 1.1 use the particle filter instead of KF or other algorithms.

Correct beacon distance estimation from RSSI values depends on the precise calibration of the path loss parameters. In order to simplify the calibration, a differential RSSI (DRSSI) approach, described e.g. in [14], could be used. With the DRSSI approach, only the path loss exponent γ needs to be identified.

The formation control algorithm is another part which could be improved. When the formation moves in a straight line towards the localized beacon,

the measured AoA data are not very variable and the beacon distance is therefore determined mostly from the RSSI data. A more advanced path planning algorithm could provide more variable AoA data on the way to the beacon and therefore accelerate the localization process.

In order to better test the performance of the algorithm before deploying it to real hardware, the simulation could be improved by incorporating a radiation pattern simulation which shape would depend on the vertical angle and the distance between the RF beacon and the antenna. That way, the influence of AoA uncertainty estimation could be tested in simulations.

Bibliography

[1] M. Vrba, *Active Searching of RFID Chips by a Group of Relatively Stabilized Helicopters*. Bachelor thesis, May 2016.

[2] J. Pogran, *Decentralized localization of active RFID transmitters by a group of unmanned aerial vehicles*. Bachelor thesis, 2017.

[3] M. Vrba, V. Spurny, M. Saska, J. Pogran, and V. Pritzl, "Localization of transmission sources using a formation of micro aerial vehicles," *Under review of IEEE Robotics and Automation Letter*, p. 8, 2018.

[4] M. Saska, J. S. Mejía, D. M. Stipanović, V. Vonásek, K. Schilling, and L. Přeučil, "Control and navigation in manoeuvres of formations of unmanned mobile vehicles," *European Journal of Control*, vol. 19, pp. 157–171, Mar. 2013.

[5] M. Saska, V. Vonásek, T. Krajník, and L. Přeučil, "Coordination and navigation of heterogeneous MAV–UGV formations localized by a 'hawk-eye'-like approach under a model predictive control scheme," *The International Journal of Robotics Research*, vol. 33, pp. 1393–1412, Sept. 2014.

[6] T. Krajník, M. Nitsche, J. Faigl, P. Vaněk, M. Saska, L. Přeučil, T. Duckett, and M. Mejail, "A Practical Multirobot Localization System," *Journal of Intelligent & Robotic Systems*, vol. 76, pp. 539–562, Dec. 2014.

[7] J. Faigl, T. Krajnik, J. Chudoba, L. Preucil, and M. Saska, "Low-cost embedded system for relative localization in robotic swarms," in *IEEE International Conference on Robotics and Automation*, pp. 993–998, IEEE, May 2013.

[8] G. Greco, C. Lucianaz, S. Bertoldo, and M. Allegretti, "Localization of RFID tags for environmental monitoring using UAV," pp. 480–483, IEEE, Sept. 2015.

[9] N. Wagle and E. Frew, "A Particle Filter Approach to WiFi Target Localization," American Institute of Aeronautics and Astronautics, Aug. 2010.

[10] M. Carpin, S. Rosati, M. E. Khan, and B. Rimoldi, "UAVs using Bayesian Optimization to Locate WiFi Devices," p. 5, 2015.

[11] F. Koohifar, I. Guvenc, and M. L. Sichitiu, "Autonomous Tracking of Intermittent RF Source Using a UAV Swarm," *arXiv:1801.02478 [cs, eess]*, Jan. 2018. arXiv: 1801.02478.

[12] J. T. Isaacs, F. Quitin, L. R. Garcia Carrillo, U. Madhow, and J. P. Hespanha, "Quadrotor control for RF source localization and tracking," pp. 244–252, IEEE, May 2014.

[13] D. JEONG and K. LEE, "Directional RSS-Based Localization for Multi-Robot Applications," *Communications and Signal Processing*, p. 7, 2013.

[14] S. M. M. Dehghan, M. Farmani, and H. Moradi, "Aerial localization of an RF source in NLOS condition," in *IEEE International Conference on Robotics and Biomimetics*, pp. 1146–1151, IEEE, Dec. 2012.

[15] S. M. M. Dehghan and H. Moradi, "A Multi-Step Gaussian Filtering Approach to Reduce the Effect of Non-Gaussian Distribution in Aerial Localization of an RF Source in NLOS Condition," in *RSIIISM International Conference on Robotics and Mechatronics*, p. 6, 2013.

[16] F. Fletcher, Branko Ristic, and Darko Musicki, "Recursive estimation of emitter location using TDOA measurements from two UAVs," pp. 1–8, IEEE, 2007.

[17] S. C. Lee, W. R. Lee, and K. H. You, "TDoA based UAV Localization using Dual-EKF Algorithm," *International Journal of Control and Automation*, vol. 2, no. 4, p. 8, 2009.

[18] D. H. Kim, K. Lee, M. Y. Park, and J. Lim, "UAV-Based Localization Scheme for Battlefield Environments," in *MILCOM 2013 - 2013 IEEE Military Communications Conference*, pp. 562–567, Nov. 2013.

[19] V. Spurný, T. Báča, M. Saska, R. Pěnička, T. Krajník, J. Thomas, D. Thakur, G. Loianno, and V. Kumar, "Cooperative Autonomous Search, Grasping and Delivering in a Treasure Hunt Scenario by a Team of UAVs," *Under review of Journal of Field Robotics*, p. 35, 2018.

[20] G. Loianno, V. Spurny, J. Thomas, T. Baca, D. Thakur, D. Hert, R. Penicka, T. Krajnik, A. Zhou, A. Cho, M. Saska, and V. Kumar, "Localization, Grasping, and Transportation of Magnetic Objects by a

team of MAVs in Challenging Desert like Environments," *IEEE Robotics and Automation Letters*, p. 8, 2018.

[21] T. Baca, G. Loianno, and M. Saska, "Embedded model predictive control of unmanned micro aerial vehicles," in *21st International Conference on Methods and Models in Automation and Robotics (MMAR)*, pp. 992–997, IEEE, Aug. 2016.

[22] V. Spurny, T. Baca, and M. Saska, "Complex manoeuvres of heterogeneous MAV-UGV formations using a model predictive control," in *21st International Conference on Methods and Models in Automation and Robotics (MMAR)*, pp. 998–1003, IEEE, Aug. 2016.

[23] T. Baca, D. Hert, G. Loianno, M. Saska, and V. Kumar, "Model Predictive Trajectory Tracking and Collision Avoidance for Reliable Outdoor Deployment of Unmanned Aerial Vehicles," *Under review of IEEE Robotics and Automation Letters*, p. 8, 2018.

[24] R. Jain, "Channel Models - A Tutorial," *WiMAX Forum AATG*, p. 21, Feb. 2007.

[25] C. A. Balanis, *Antenna theory: analysis and design*. Hoboken, NJ: John Wiley, 3rd ed ed., 2005.

[26] W. H. Press, S. H. Teukolsky, W. T. Vetterling, and B. P. Flannery, *Numerical recipes - The Art of Scientific Computing*. Cambridge University Press, third ed., 2007.

[27] G. Welch and G. Bishop, "An Introduction to the Kalman Filter," p. 81, 2001.

[28] S. D. Gupta, J. Y. Yu, M. Mallick, M. Coates, and M. Morelande, "Comparison of angle-only filtering algorithms in 3d using EKF, UKF, PF, PFF, and ensemble KF," in *2015 18th International Conference on Information Fusion (Fusion)*, pp. 1649–1656, July 2015.

[29] A. Giannitrapani, N. Ceccarelli, F. Scortecci, and A. Garulli, "Comparison of EKF and UKF for Spacecraft Localization via Angle Measurements," *IEEE Transactions on Aerospace and Electronic Systems*, vol. 47, pp. 75–84, Jan. 2011.

[30] X. b. Jin, Y. Shi, and N. Chun-Xue, "Tracking for indoor RFID system with UKF and EKF," in *2015 International Conference on Estimation, Detection and Information Fusion (ICEDIF)*, pp. 146–151, Jan. 2015.

[31] T. Nick, J. Goetze, W. John, and G. Stoenner, "Comparison of extended and Unscented Kalman Filter for localization of passive UHF RFID labels," in *2011 XXXth URSI General Assembly and Scientific Symposium*, pp. 1–4, Aug. 2011.

[32] S. J. Julier and J. K. Uhlmann, "A New Extension of the Kalman Filter to Nonlinear Systems," pp. 182–193, 1997.

[33] R. R. Labbe Jr, "Kalman and Bayesian Filters in Python," p. 491, 2015.

[34] T. Bailey, B. Upcroft, and H. Durrant-Whyte, "Validation Gating for Non-Linear Non-Gaussian Target Tracking," in *2006 9th International Conference on Information Fusion*, pp. 1–6, July 2006.

Appendix A

CD contents

The contents of the CD attached to this thesis are listed in table A.1.

Directory	Content
sources	software source code
thesis	thesis in pdf format
videos	videos of performed experiments

Table A.1: CD contents

Appendix B

List of abbreviations

The abbreviations used in this thesis are listed in Table B.1.

Abbreviation	Meaning
RF	radio frequency
MAV	micro aerial vehicle
UAV	unmanned aerial vehicle
UKF	unscented kalman filter
EKF	extended kalman filter
KF	kalman filter
AoA	angle of arrival
RSSI	received signal strength indication
RFID	radio frequency identification
GPS	global positioning system
TDoA	time difference of arrival
GNSS	global navigation satellite system
MPC	model predictive control
RTK	real-time kinematic
NEES	normalized estimation error squared
RMSE	root mean square error
DRSSI	differential received signal strength indication

Table B.1: List of abbreviations